Inorganic Chemistry

ARTICLE

pubs.acs.org/IC

Structure and Photoluminescence Tuning Features of Mn^{2+}- and Ln^{3+}-Activated Zn-Based Heterometal−Organic Frameworks (MOFs) with a Single 5-Methylisophthalic Acid Ligand

Qi-Bing Bo,*[,†] Hong-Yan Wang,[†] Da-Qi Wang,[‡] Zhen-Wei Zhang,[†] Jin-Ling Miao,[†] and Guo-Xin Sun[†]

[†]School of Chemistry and Chemical Engineering, University of Jinan, Jinan 250022, China

[‡]College of Chemistry and Chemical Engineering, Liaocheng University, Liaocheng 252059, China

Supporting Information

ABSTRACT: In attempts to investigate whether the photoluminescence properties of the Zn-based heterometal−organic frameworks (MOFs) could be tuned by doping different Ln^{3+} (Ln = Sm, Eu, Tb) and Mn^{2+} ions, seven novel 3D homo- and hetero-MOFs with a rich variety of network topologies, namely, $[Zn(mip)]_n$ (**Zn−Zn**), $[Zn_2Mn(OH)_2(mip)_2]_n$ (**Zn−Mn**), $[Mn_2Mn(OH)_2(mip)_2]_n$ (**Mn−Mn**), $[ZnSm(OH)(mip)_2]_n$ (**Zn−Sm**), $[ZnEu(OH)(mip)_2]_n$ (**Zn−Eu1**), $[Zn_5Eu(OH)(H_2O)_3(mip)_6\cdot(H_2O)]_n$ (**Zn−Eu2**), and $[Zn_5Tb(OH)(H_2O)_3(mip)_6]_n$ (**Zn−Tb**), (mip = 5-methylisophthalate dianion), have been synthesized hydrothermally based on a single 5-methylisophthalic acid ligand. All compounds are fully structurally characterized by elemental analysis, FT-IR spectroscopy, TG-DTA analysis, single-crystal X-ray diffraction, and X-ray powder diffraction (XRPD) techniques. The various connectivity modes of the mip linkers generate four types of different structures. Type I (**Zn−Zn**) is a 3D homo-MOF with helical channels composed of $Zn_2(COO)_4$ SBUs (second building units). Type II (**Zn−Mn** and **Mn−Mn**) displays a nest-like 3D homo- or hetero-MOF featuring window-shaped helical channels composed of $Zn_4Mn_2(OH)_4(COO)_8$ or $Mn_4Mn_2(OH)_4(COO)_8$ SBUs. Type III (**Zn−Sm** and **Zn−Eu1**) presents a complicated corbeil-like 3D hetero-MOF with irregular helical channels composed of $(SmZnO)_2(COO)_8$ or $(EuZnO)_2(COO)_8$ heterometallic SBUs. Type IV (**Zn−Eu2** and **Zn−Tb**) contains a heterometallic SBU $Zn_5Eu(OH)(COO)_{12}$ or $Zn_5Tb(OH)(COO)_{12}$, which results in a 3D hetero-MOF featuring irregular channels impregnated by parts of the free and coordinated water molecules. Photoluminescence properties indicate that all of the compounds exhibit photoluminescence in the solid state at room temperature. Compared with a broad emission band at ca. 475 nm (λ_{ex} = 380 nm) for **Zn−Zn**, compound **Zn−Mn** exhibits a remarkably intense emission band centered at 737 nm (λ_{ex} = 320 nm) due to the characteristic emission of Mn^{2+}. In addition, the fluorescence intensity of compound **Zn−Mn** is stronger than that of **Mn−Mn** as a result of Zn^{2+} behaving as an activator for the Mn^{2+} emission. Compound **Zn−Sm** displays a typical Sm^{3+} emission spectrum, and the peak at 596 nm is the strongest one (λ_{ex} = 310 nm). Both **Zn−Eu1** and **Zn−Eu2** give the characteristic emission transitions of the Eu^{3+} ions (λ_{ex} = 310 nm). Thanks to the ambient different crystal-field strengths, crystal field symmetries, and coordinated bonds of the Eu^{3+} ions in compounds **Zn−Eu1** and **Zn−Eu2**, the spectrum of the former compound is dominated by the $^5D_0 \rightarrow {}^7F_2$ transition (612 nm), while the emission of the $^5D_0 \rightarrow {}^7F_4$ transition (699 nm) for the latter one is the most intense. Compound **Zn−Tb** emits the characteristic Tb^{3+} ion spectrum dominated by the $^5D_4 \rightarrow {}^7F_5$ (544 nm) transition. Upon addition of the different activated ions, the luminescence lifetimes of the compounds are also changed from the nanosecond (**Zn−Zn**) to the microsecond (**Zn−Mn**, **Mn−Mn**, and **Zn−Sm**) and millisecond (**Zn−Eu1**, **Zn−Eu2**, and **Zn−Tb**) magnitude orders. The structure and photoluminescent property correlations suggest that the presence of Mn^{2+} and Ln^{3+} ions can activate the Zn-based hetero-MOFs to emit the tunable photoluminescence.

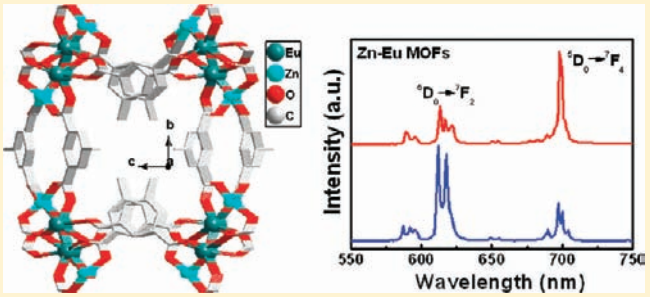

INTRODUCTION

It is known that doped inorganic materials with different activating metal ions can tune the luminescent properties of the host materials to a large extent through changing the electronic structure. Among them, considerable attention has been paid to the study of the photoluminescence properties of Zn-based inorganic host materials doped by RE^{3+} (rare earth ions) because of the efficient energy transfer leading to sensitized luminescence from the lanthanide ions. For instance, ZnO,[1] ZnS,[2] and $SrZnO_2$[3] doped with RE^{3+} exhibit different color outputs. On the other hand, as an alternative to RE^{3+}, Mn^{2+} has also been intensively studied as an optically active emission center in Zn-based host materials due to the fact that tetrahedrally and

Received: May 26, 2011
Published: September 16, 2011

dx.doi.org/10.1021/ic201124c | *Inorg. Chem.* 2011, 50, 10163–10177

Scheme 1. Diverse Coordination Modes of mip (mip = 5-methylisophthalate dianion)

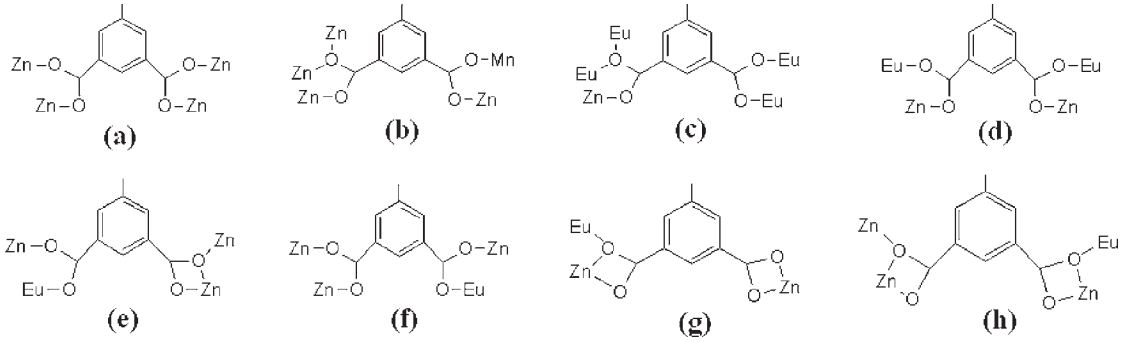

octahedrally coordinated Mn^{2+} ions usually give green to yellow and orange to deep red emissions, respectively.[4] Of which, ZnO,[5] ZnS,[6] ZnSe,[7] ZnTe,[8] Zn_2SiO_4,[9] and BaZnOS[10] have been reported to be good host materials for Mn^{2+} luminescence. Apart from these, there are several reports on the photoluminescence properties of double-ion-codoped Zn-based inorganic host materials like (Eu^{3+}, Mn^{2+}):$BaZnSiO_4$,[11] (Cd^{2+}, Mn^{2+}):ZnS,[12] (Tb^{3+}, Mn^{2+}):$ZnSrPO_4$,[13] and (Ba^{2+}, Mn^{2+}):$SrZnO_2$.[14] Studies show that the doping or codoping of metal ions can induce more mismatches and defects in the lattice structure and further exhibit interesting and highly diversified luminescence properties which strongly depend on the nature of the dopant ions.

Recently, it was noticed that Mn^{2+}-doped Zn-based host materials can be further incorporated into other inorganic matrixes (via site substitution of different cations) or organic ligands (via the covalence between dopant ion and ligands) resulting in core/shell microcrystals[15] or inorganic−organic hybrid materials,[16] respectively. Photoluminescence properties of theses samples show that the different doping content of Mn can tune the emission band positions, luminescence efficiency, and brightness of the emission from Mn^{2+} in the Zn-based host materials thanks to the activator role of Zn^{2+}.

On the other hand, numerous Zn-based MOFs with different organic ligands are known to exhibit a large variety of coordination geometries and intense photoluminescence at room temperature.[17] However, they invariably exhibit typical blue and green emission attributed to the ligand-to-ligand charge-transfer (LLCT) or ligand-to-metal charge-transfer (LMCT) states.[18] At the same time, three 3D anionic hetero-MOFs with 1D channels, $\{K_5[Ln_5(IDC)_4(ox)_4]\}_n \cdot (20H_2O)_n$ (IDC = imidazole-4,5-dicarboxylate, ox = oxalate), were reported by T.-B. Lu. The luminescent properties show that they can be modified through the exchange of guest K^+ with various cations and have potential as tunable lanthanide luminescent materials.[19]

We wonder whether the photoluminescence properties of Zn-based MOFs could be conveniently tuned by incorporating RE^{3+} and Mn^{2+} ions into them, similar to the Zn-based inorganic host materials or inorganic−organic hybrid materials mentioned above. If so, many hetero-MOFs with special photoluminescence properties might form. Therefore, our research interest has been focused on the synthesis, structure, and photoluminescence tuning features of Mn^{2+}- and Ln^{3+}-activated Zn-based hetero-metal−organic frameworks.

To date, there are many reports about the luminescent properties of Zn−Ln MOFs. From a structural point of view, most of them use Schiff base ligands to bind both Zn^{2+} and Ln^{3+} ions.[20] Occasionally, parts of them are synthesized by single organic ligands containing both N- and O-donor atoms, such as imidazole−dicarboxylic acid[21] or pyridine−dicarboxylic acid.[22] Furthermore, in order to meet the high-coordination-number requirement of lanthanide ions and construct novel structural topologies, a lot of mixed organic ligands with N- or O-donor atoms can also be employed in construction of Zn−Ln MOFs.[23]

However, except for Zn−Ln MOFs with a single aromatic carboxylic acid (such as oxidiacetic acid[24] and chelidamic acid[25]), which mainly focus on studying the adsorption or magnetic properties, luminescent Zn−Ln MOFs constructed by single aromatic carboxylic acid are scarce and we find only one previously reported on the Zn−Eu and Zn−Tb MOFs with α-furancarboxylic acid as an organic ligand.[26] Similarly, in comparison with the reported Zn−Ln MOFs, although some of the Zn−Mn MOFs have been reported, such as $MnZn_2(crot)_6(base)_2$[27] (crot = crotonate, base = quinoline), $LZn_2Mn(OAc)_2(MeOH)_2$ and $(2pmoap\text{-}2H)_6Mn_5Zn_4$[28] (2pmoap-2H = ditopic and tritopic hydrazone), $Mn_3Zn_2(Rsalox)_3O(N_3)_6X_2$[29] (R = H or Me, salox = salicylaldoximes), $Mn_3Zn(hmp)_3O(N_3)_3(C_3H_5O_2)_3$[30] (hmp = 2-pyridinemethanol), $(NEt_4)_3(Mn_3Zn_2(salox)_3O(N_3)_6X_2)$[31] (salox = salicylaldoximes), and $(Zn_3Mn_{1.5}(bpe)(bba)_4(Hbba)) \cdot bpe$[32] (bpe = 1,2-bis(4-pyridyl)ethane, H_2bba = benzene-1,3-biscarboxylic acid), the photoluminescence properties originated from Mn^{2+} emission have not been reported so far except for the novel structure and magnetic properties. Even as different kinds of Mn-based MOFs like $(Mn(tren))_2(\mu_2\text{-}Ge_2S_6)$[33] (tren = *N*,*N*,*N*-tris(2-aminoethyl)amine), $(Mn(dien)_2)(Mn(dien)AsS_4)_2 \cdot 4H_2O$ (dien = diethyleneamine), $(Mn(en)_3)_2(Mn(en)_2AsS_4)(As_3S_6)$[34] (en = ethyleneamine), $Mn(2,2'\text{-bipy})_2S_6$[35] (2,2′-bipy = 2,2′-bipyridyl), $Mn_2(Htmopa)_4(H_2O)_4$[36] (Htmopa = 2,3,6,7-tetramethoxyphenanthrene-9-carboxylic acid), *tcc*-$LMnCl_2 \cdot 0.5H_2O$,[37] $(Mn_3(2,2'\text{-bipy})_3(AsS_4)_2) \cdot H_2O$, and $Mn_2(2,2'\text{-bipy})As_2S_5$[38] have been obtained, their photoluminescence invariably show the characteristic emission attributed to intraligand (IL) or ligand-to-ligand charge-transfer (LLCT) states, not to Mn^{2+}-centered emission.

Also, noticeably, in contrast to single aromatic carboxylic acid ligands, like oxidiacetic acid,[24] chelidamic acid,[25] and α-furancarboxylic acid[26] mentioned above, 5-methylisophthalic acid not only contains two potential bridging carboxylate moieties but also possesses the electron-donating $-CH_3$ substituents; the steric hindrance of the $-CH_3$ group in the bridging ligands can greatly reduce interpenetrating of MOFs. Therefore, many of the Zn-based homo-MOFs with 5-methylisophthalic acid ligand or its derivatives have been synthesized and their photoluminescence properties also reported.[18g,39] However, to the best of our

dx.doi.org/10.1021/ic201124c |*Inorg. Chem.* 2011, 50, 10163–10177

Table 1. Crystal Data and Refinement Parameters for Zn−Zn, Zn−Mn, and Mn−Mn

compound	Zn−Zn	Zn−Mn	Mn−Mn
empirical formula	$C_9H_6O_4Zn$	$C_{18}H_{14}O_{10}Zn_2Mn$	$C_{18}H_{14}O_{10}Mn_3$
fw	243.51	575.97	555.11
cryst syst	monoclinic	monoclinic	monoclinic
space group	$P2_1/c$	$C2/c$	$C2/c$
a/Å	4.5796 (2)	19.6382(19)	19.862(2)
b/Å	12.1184 (5)	17.2833(12)	17.2802(18)
c/Å	15.2298 (6)	5.2217(4)	5.2868(6)
α/deg	90	90	90
β /deg	94.195(4)	92.183(8)	90.724(11)
γ/deg	90	90	90
volume/ Å^3	842.95 (6)	1771.0(3)	1814.4(3)
Z	4	4	4
ρ_{calcd}/g·cm^{-3}	1.919	2.160	2.032
μ /mm^{-1}	2.893	3.451	2.117
F (000)	488	1148	1108
reflns collected	6760	5212	13 125
unique reflns	1646	1733	1761
R_{int}	0.0287	0.0447	0.0992
GOF	1.027	1.081	1.083
R_1 ($I > 2\sigma(I)$)	0.0287	0.0499	0.0546
wR_2 ($I > 2\sigma(I)$)	0.0789	0.1433	0.1367
R_1 (all data)	0.0348	0.0612	0.0576
wR_2 (all data)	0.0804	0.1495	0.1380

knowledge, reports of Zn-based hetero-MOFs activated by transition metal ions and rare earth ions have not been studied so far.

Inspired by the aforementioned considerations, the aim of our research is to find novel Zn-based MOFs used as matrixes similar with Zn-based inorganic host materials or inorganic−organic hybrid materials. In addition, different activated ions can be structurally incorporated into them, resulting in tunable luminescent properties of Zn-based hetero-MOFs. In this contribution, we present the synthesis, characterization, and photoluminescence properties of four kinds of seven novel $[Zn(mip)]_n$ (**Zn−Zn**), $[Zn_2Mn(OH)_2(mip)_2]_n$ (**Zn−Mn**), $[Mn_2Mn(OH)_2(mip)_2]_n$ (**Mn−Mn**), $[ZnSm(OH)(mip)_2]_n$ (**Zn−Sm**), $[ZnEu(OH)(mip)_2]_n$ (**Zn−Eu1**), $[Zn_5Eu(OH)(H_2O)_3(mip)_6\cdot(H_2O)]_n$ (**Zn−Eu2**), and $[Zn_5Tb(OH)(H_2O)_3(mip)_6]_n$ (**Zn−Tb**) (mip = 5-methylisophthalate dianion) mono- and hetero-MOFs with single 5-methylisophthalic acid ligand. Our studies indicate that the photoluminescence properties of the **Zn−Mn** and **Zn−Ln** (Ln = Sm, Eu, Tb) hetero-MOFs can be tuned by the corresponding activated ion emission.

RESULTS AND DISCUSSION

Description of Crystal Structures. Single-crystal X-ray diffraction reveals that seven novel compounds **Zn−Zn**, **Zn−Mn**, **Mn−Mn**, **Zn−Sm**, **Zn−Eu1**, **Zn−Eu2**, and **Zn−Tb** possess four kinds of structures. Eight types of mip coordination modes can be found in Scheme 1. The crystallographic data and structure refinement details for all compounds are depicted in Tables 1 and 2. Selected bond distances and angles for all compounds are listed in Tables S1−S7 in the Supporting Information.

Crystal Structure of $[Zn(mip)]_n$ (Zn−Zn). The crystal structure of **Zn−Zn** is composed of one Zn atom and one mip ligand in each independent crystallographic unit. As shown in Scheme 1a and Figure S1, Supporting Information, each mip ligand links four Zn atoms using its two μ_2-η^1:η^1-bridging carboxylate groups and each Zn atom is tetrahedrally coordinated to four O atoms from four mip ligands with Zn−O bond lengths ranging from 1.9226(18) to 1.9637(19) Å. It is noteworthy that two symmetry-related zinc atoms [Zn1···Zn1D = 3.5621(4) Å], two carboxylate groups, and four half ones constitute a 4-connected SBU (second building unit) $Zn_2(COO)_4$ (Figure 1a). Pairs of the neighboring half carboxylate groups (O−C8−O) in the SBU coordinate to Zn atoms first and give rise to the left- and right-handed helical chains along the a axis (Figure 1c). Then, all of the helical chains are further cross-linked by other carboxylate groups (O−C9−O) of mip ligands into an overall 3D MOF with 1D helical channels extending along the crystallographic a axis as shown in Figure 1b. It is evident that the channels are hydrophobic, and their cross sections give an array of the irregular 4^4 brick-like net pores in the bc crystallographic plane. Furthermore, if the mip ligand and two symmetry-related zinc atoms of the SBU are considered as two kinds of nodes, the 3D framework of **Zn−Zn** can be simplified in a binodal (4,8)-connected **scu** topology with its Schlafli symbol being $(4^{16}.6^{12})$ $(4^4.6^2)_2$ as shown in Figure 2.

Crystal Structure of $[Zn_2Mn(OH)_2(mip)_2]_n$ (Zn−Mn). Since single-crystal X-ray diffraction analysis reveals that compounds **Zn−Mn** and **Mn−Mn** possess essentially the same structures, herein we limit the description of crystal structures to that of **Zn−Mn**, which crystallizes in the monoclinic space group $C2/c$. Figure S2, Supporting Information, shows the coordination environment of the mip ligand and Zn and Mn atoms. It is evident that each mip ligand adopts a μ_5-bridge linking mode, where mip acts as a bridging ligand to link one manganese and four zinc atoms simultaneously with carboxylate groups adopting μ_2-η^1:η^1-bridging and μ_3-η^2:η^1-bridging coordination modes (Scheme 1b). Each zinc center has a square-pyramidal coordination environment and is coordinated by five carboxylate oxygen donors. One (O5) originates from a triple-bridging hydroxyl group, while the other four (O2, O3A, O3B, and O4) come from four different mip ligands. The Zn−O bond lengths fall in the range 2.0168(3)−2.1730(3) Å. In addition, each manganese atom is six coordinated by two carboxylate oxygen donors (O1 and O1D) of two different mip groups and four oxygen atoms (O5, O5B, O5C, and O5D) of four hydroxyl groups, generating a distorted octahedral coordination arrangement with the Mn−O bond length ranging from 2.1917(3) to 2.2553(3) Å. Compared to compound **Zn−Zn**, two symmetry-related Mn atoms (Mn1 and Mn1C) and four Zn atoms [Zn1···Zn1E = 3.3892(8) Å, Zn1···Mn1 = 3.3226(7) Å, Mn1···Mn1C = 3.3091(8) Å] in **Zn−Mn** share eight carboxylate groups of mip ligands and four hydroxyl groups to give a linear manganese-centered hexanuclear heterometallic SUB (Figure 3a). It is evident that the heterometallic SUB is composed of four carboxylate groups (−O−C8−O−) and eight half ones (−O−C9−O−), constituting a 12-connected SBU $Zn_4Mn_2(OH)_4(COO)_8$. Each SBU is further connected to four neighboring ones to form a nest-like 3D structure (Figure 3b). The adjacent carboxylate groups (O−C8−O and O−C9−O) in the SBUs coordinate to Zn atoms first generating a 1D double-helical chain with the left- and right-handed

dx.doi.org/10.1021/ic201124c |Inorg. Chem. 2011, 50, 10163–10177

Table 2. Crystal Data and Refinement Parameters for Zn−Sm, Zn−Eu1, Zn−Eu2, and Zn−Tb.

compound	Zn−Sm	Zn−Eu1	Zn−Eu2	Zn−Tb
empirical formula	$C_{18}H_{13}O_9$ ZnSm	$C_{18}H_{13}O_9ZnEu$	$C_{54}H_{45}O_{29}Zn_5Eu$	$C_{54}H_{43}O_{28}Zn_5Tb$
fw	589.00	590.61	1636.71	1625.65
cryst syst	orthorhombic	orthorhombic	triclinic	triclinic
space group	*Pnma*	*Pnma*	*P*-1	*P*-1
a/Å	7.2480(3)	7.2231(5)	13.2812(11)	13.3015(5)
b/Å	24.9022(15)	24.777(2)	15.1611(13)	15.1095(6)
c/Å	20.3892(12)	20.3178(19)	15.6701(9)	15.6882(6)
α/deg	90	90	100.758(6)	100.837(3)
β/deg	90	90	100.424(6)	100.171(3)
γ/deg	90	90	108.033(8)	108.559(3)
volume/ Å^3	3680.1(3)	3636.2(5)	2849.7(4)	2839.47(19)
Z	8	8	2	2
ρ_{cal} /g·cm^{-3}	2.126	2.158	1.907	1.901
μ /mm^{-1}	4.515	4.789	3.249	3.399
F (000)	2280	2288	1628	1612
reflns collected	11 578	22 502	35 372	35 218
unique reflns	3657	3770	11 617	11 578
R_{int}	0.0389	0.0460	0.0470	0.0289
GOF	1.068	1.047	1.052	1.039
R_1 ($I > 2\sigma(I)$)	0.0414	0.0247	0.0353	0.0248
wR_2 ($I > 2\sigma(I)$)	0.0957	0.0501	0.0743	0.0566
R_1 (all data)	0.0498	0.0325	0.0518	0.0323
wR_2 (all data)	0.1006	0.0522	0.0829	0.0603

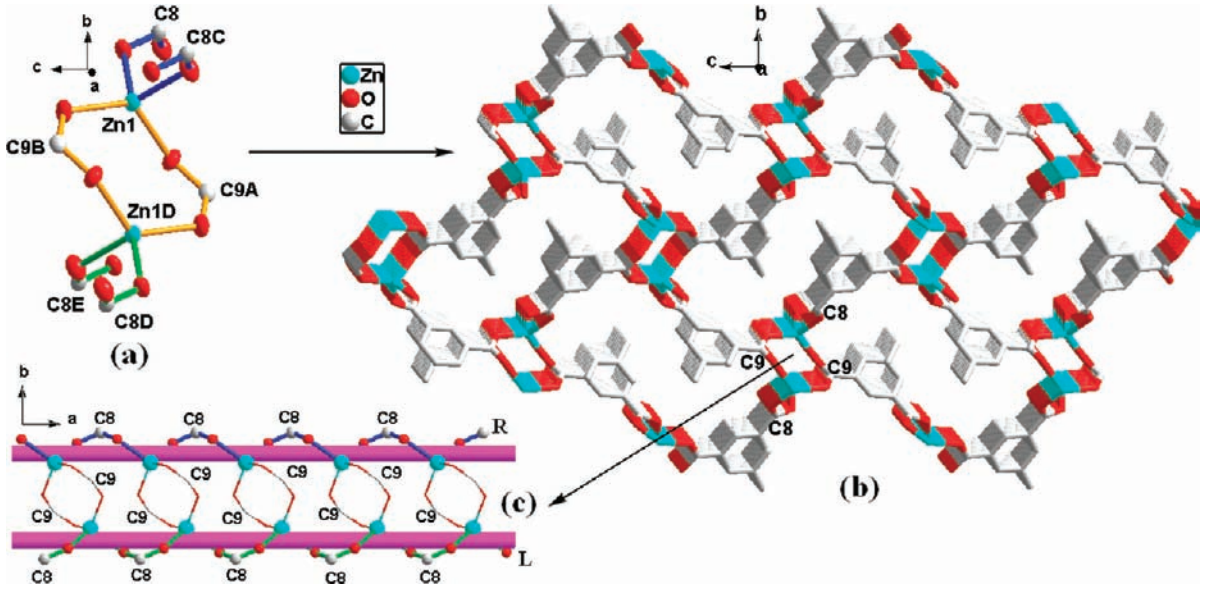

Figure 1. (a) 4-connected $Zn_2(COO)_4$ SBUs are shown as thermal ellipsoids (50% probability level) for **Zn−Zn**. (b) 3D MOFs with helical channels for **Zn−Zn**. (c) Double-helical chains with the right-hand (R) and left-hand helices (L) for **Zn−Zn**. Hydrogen atoms are omitted for clarity. Symmetry codes: A ($-x$, $-0.5 + y$, $0.5 - z$), B ($1 + x$, $0.5 - y$, $0.5 + z$), C ($1 + x$, y, z), D ($1 - x$, $-y$, $1 - z$), E ($-x$, $-y$, $1 - z$).

characteristic along the *c* axis (Figure 3d). At the same time, the hydroxyl groups coordinate to the Mn atoms, giving rise to another similar chain (Figure 3c). Then, all of the 1D double helical chains are cross-linked by the carboxylate groups (−O−C8-O-) of mip ligands into a 3D hetero-MOF featuring window-shaped helical channels with cross-section dimensions of 15.4720(2) × 13.4807(2) Å and 7.4347(9) × 3.2480(8) Å in the *ab* plane, as shown in Figure S3, Supporting Information. Of particular interest, there are no free guest water molecules residing in the helical channels and no evidence of hydrogen-bond interactions in the structure of **Zn−Mn**. Therefore, the 3D supramolecular frameworks in **Zn−Mn** are only stabilized by the covalent bonding interactions and $\pi\cdots\pi$ stacking interactions of the two phenyl rings of mip ligands.

dx.doi.org/10.1021/ic201124c |*Inorg. Chem.* 2011, 50, 10163–10177

Topologically, using the mip ligand and the $Zn_4Mn_2(OH)_4$ unit as nodes, the 3D structure of Zn−Mn can also be simplified into a previously unknown (4,8)-connected 2-nodal network with $(4^{13}.6^{14}.8)$ $(4^4.6^2)_2$ topology, as shown in Figure 4.

Crystal Structure of $[ZnEu(OH)(mip)_2]_n$(Zn−Eu1). Single-crystal X-ray diffraction study reveals that compounds **Zn−Sm** and **Zn−Eu1** are isomorphous and crystallized in the orthorhombic system with space group *Pnma*. Therefore, only the structure of compound **Zn−Eu1** is described in detail. As shown in Figure S4, Supporting Information, the asymmetric unit of **Zn−Eu1** contains one crystallographically independent Zn atom, one Eu atom, one hydroxyl group, and two mip ligands. In addition, the independent Zn atom is coordinated in a tetrahedral geometry by three carboxylic oxygen atoms from three mip ligands and one hydroxyl oxygen atom with the Zn−O bond length ranging from 1.9279(15) to 1.9560(13) Å. The Eu atom is surrounded by eight oxygen atoms from six mip ligands and two hydroxyl groups, exhibiting a bicapped trigonal prismatic coordination geometry. The Eu−O bond lengths range from 2.3235(15) to 2.7126(12) Å. Furthermore, two types of coordination modes of the mip ligands are also found. One acts as a bridging ligand to link one Zn and four Eu atoms simultaneously with carboxylate groups adopting μ_2-η^1:η^1-bridging and μ_3-η^2:η^1-bridging coordination modes (Scheme 1c); the other links two Zn and Eu atoms adopting two μ_2-η^1:η^1-bridging ones (Scheme 1d). A further feature of **Zn−Eu1** is the presence of a centrosymmetric linear array of two symmetry-related Zn and Eu

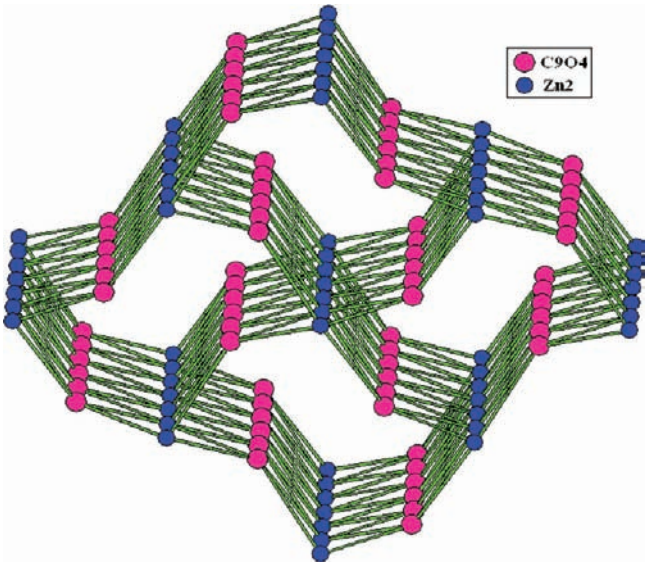

Figure 2. (4,8)-connected **scu** 3D topology framework for **Zn−Zn**.

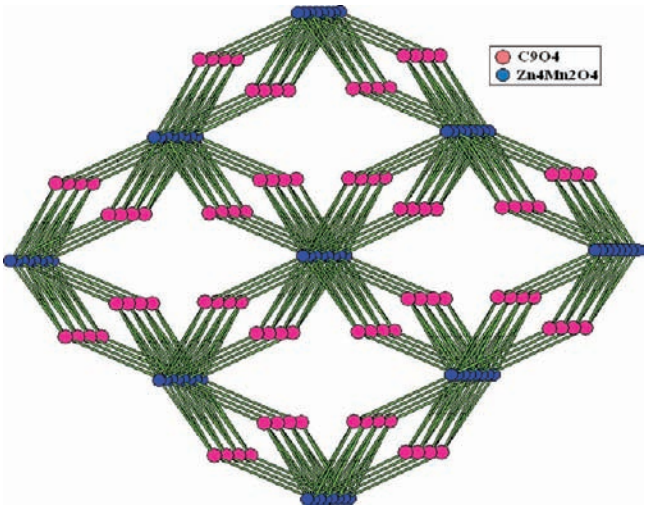

Figure 4. Previously unknown (4,8)-connected 3D topology framework for **Zn−Mn**.

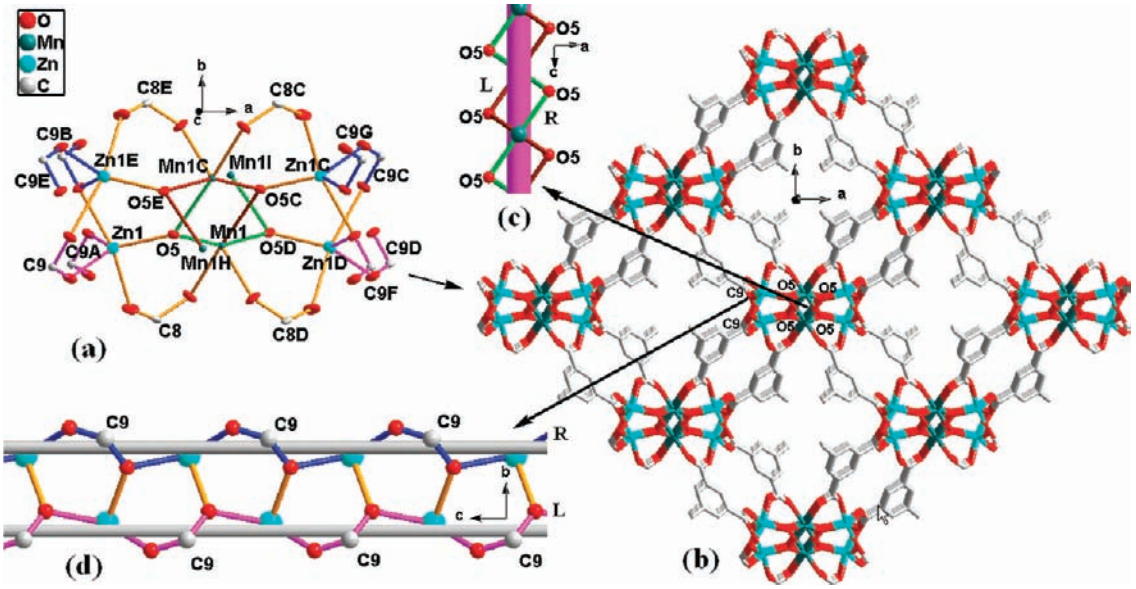

Figure 3. (a) 12-connected $Zn_4Mn_2(OH)_4(COO)_8$ SBUs are shown as thermal ellipsoids (50% probability level) for **Zn−Mn**. (b) Nest-like 3D MOFs featuring window-shaped helical channels for **Zn−Mn**. (c) Double-helical chains (containing only Mn atoms) with the right-hand (R) and left-hand helices (L) for **Zn−Mn**. (d) Double-helical chains (containing only Zn atoms) with the right-hand (R) and left-hand helices (L) for **Zn−Mn**. Hydrogen atoms are omitted for clarity. Symmetry codes: A $(x, y, -1 + z)$, B $(x, 2 - y, -0.5 + z)$, C $(2 - x, 2 - y, 1 - z)$, D $(2 - x, y, 0.5 - z)$, E $(x, 2 - y, 0.5 + z)$, F $(2 - x, y, 1.5 - z)$, G $(2 - x, 2 - y, 2 - z)$, H $(x, y, 1 + z)$, I $(2 - x, 2 - y, -z)$.

dx.doi.org/10.1021/ic201124c |*Inorg. Chem.* 2011, 50, 10163–10177

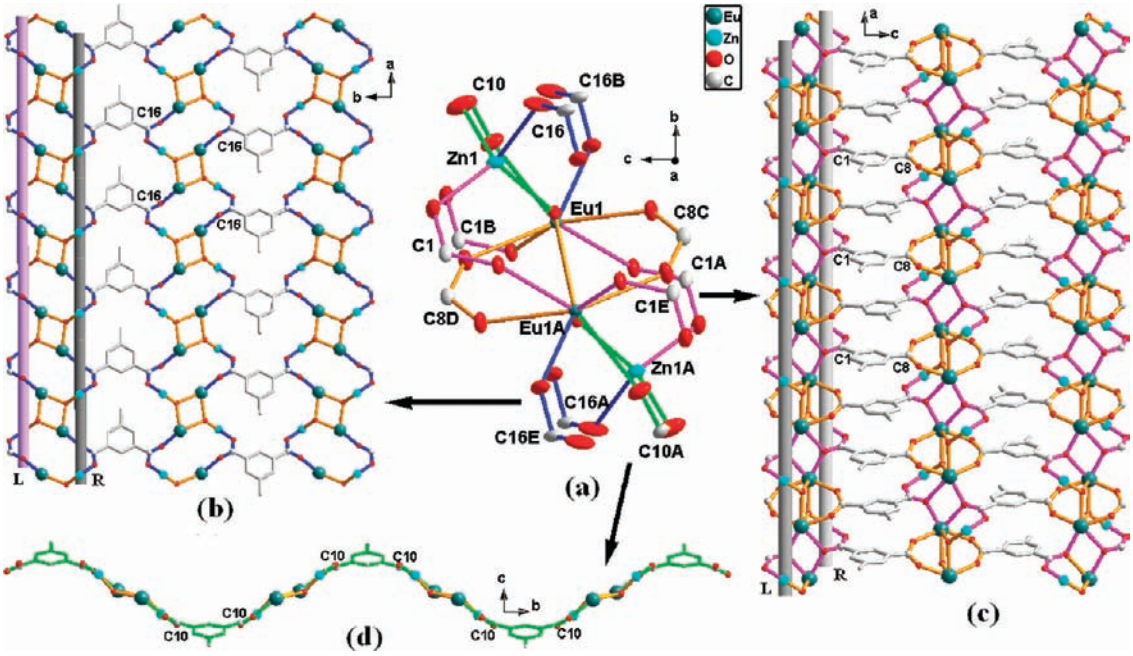

Figure 5. (a) 8-connected $(EuZnO)_2(COO)_8$ SBUs are shown as thermal ellipsoids (50% probability level) for **Zn**−**Eu1**. (b) 2D layer structure (containing only O−C16−O carboxylate group) with the left- and right-handed double-helical chains for **Zn**−**Eu1**. (c) 2D layer structure (containing both O−C1−O and O−C8−O carboxylate groups) with the left- and right-handed double-helical chains for **Zn**−**Eu1**. (d) Zig-zag-shaped chain containing only the O−C10−O carboxylate group for **Zn**−**Eu1**. Hydrogen atoms are omitted for clarity. Symmetry codes: A $(-x, 1 - y, -z)$, B $(-1 + x, y, z)$, C $(0.5 - x, 1 - y, -0.5 + z)$, D $(-0.5 + x, y, 0.5 - z)$, E $(1 - x, 1 - y, -z)$.

atoms bridged by eight carboxylate groups from mip ligands and two hydroxyl groups as shown in Figure 5a. This linear heteroquadrinuclear coordination unit, formulated as $(EuZnO)_2(COO)_8$, can be regarded as an 8-connected secondary building unit (SBU) with Zn1−Eu1, Eu1−Eu1A, and Zn1−Zn1A separations of 3.8297(3), 3.9201(2), and 6.6101(5) Å, respectively. Also noticeable is that the adjacent carboxylate groups (O−C16−O) in the SBUs coordinate to the heterometallic clusters $(EuZnO)_2$ forming one 2D layer structure with the left- and right-handed double-helical chains in the *ab* plane (Figure 5b). At the same time, the other similar 2D layer is also generated through the coordination between the carboxylate groups (O−C1−O and O−C8−O) and the $(EuZnO)_2$ clusters in the *ac* plane (Figure 5c). Furthermore, by virtue of the coordination of another carboxylate group (O−C10−O) with the EuZnO clusters, a zig-zag-shaped chain can also be formed along the *b* axis (Figure 5d). As a result, the two kinds of 2D layers mentioned above are cross-linked along the *a* axis, giving rise to a 3D framework (Figure S5, Supporting Information), which is further connected by the zig-zag chain into a complicated corbeil-like 3D framework with irregular helical channels finally, as shown in Figure 6.

Considering the mip ligand and the $Eu_2Zn_2(OH)_2$ unit as nodes, the 3D structure of **Zn**−**Eu1** can also be simplified into an unusual (2,3,10)-connected 3-nodal network with $(4^3)_2(4^8.6^6.8^{27}.12^4)(4)_2$ topology, as shown in Figure 7.

Crystal Structures of $[Zn_5Eu(OH)(H_2O)_3(mip)_6\cdot(H_2O)]_n$ (Zn−Eu2). Crystallographic analysis revealed compounds **Zn**−**Eu2** and **Zn**−**Tb** are isostructural and crystallized in the triclinic system with space group *P*-1. Therefore, only the structure of compound **Zn**−**Eu2** is described in detail. As shown in Figure 8a, the crystal structure of **Zn**−**Eu2** contains one Eu atom, five Zn atoms, one hydroxyl group, six mip ligands, three coordinated water molecules, and one free water molecule in the independent crystallographic unit. Each Eu atom is eight coordinated by six oxygen atoms from six mip ligands and two oxygen atoms from two coordinated water molecules with the Eu−O distances falling in the range 2.3278(23)−2.5563(32) Å. In addition, all zinc atoms have five types of coordination environments. Both Zn1 and Zn2 connect five carboxylate oxygen donors from four different mip anions and adopt a square pyramidal coordination mode with the average Zn−O distance being 2.0964(3) Å. Compared with Zn1 and Zn2, Zn3 is five coordinated by four oxygen atoms from three mip ligands and one oxygen atom from the hydroxyl group with the average Zn−O distance being 2.0960(3) Å. Zn4 connects one hydroxyl oxygen and five carboxylate oxygen donors from four different mip anions, resulting in an octahedral coordination arrangement with the average Zn−O distance being 2.1373(9) Å. On the other hand, Zn5 is five coordinated by three oxygen atoms from two mip ligands, one oxygen atom from the hydroxyl group, and one oxygen atom from a coordinated water molecule with the average Zn−O distance being 2.1276(5) Å. Furthermore, the subtle distinction between Zn1, Zn2, Zn3, Zn4, and Zn5 originates from four types of coordination modes of the mip ligands, as shown in Scheme 1e−h.

Figure 8b shows that the coordination unit of **Zn**−**Eu2** contains a linear array of six metal atoms bridged by 12 carboxylate groups and one hydroxyl group, which can be viewed as a heterohexanuclear SBU formulated as $Zn_5Eu(OH)(COO)_{12}$ (Zn1···Eu1 = 4.0760(7) Å, Eu1···Zn2 = 4.0033(6) Å, Zn2···Zn3 = 4.0242(7) Å, Zn3···Zn4 = 3.0677(6) Å, Zn4···Zn5 = 3.3857(7) Å, Zn3···Zn5 = 3.3872(7) Å). The SBUs are interconnected to each other, forming a complicated 3D structure. The heterohexanuclear metallic cluster $Zn_5Eu(OH)$ is fist extended through eight carboxylate groups from four mip ligands

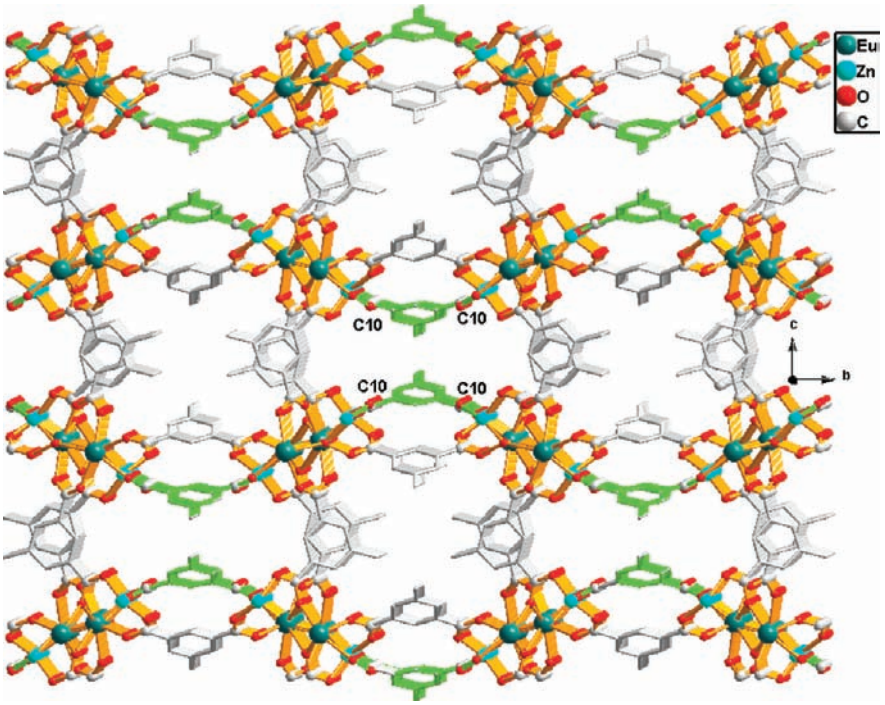

Figure 6. Corbeil-like 3D framework with irregular helical channels for **Zn−Eu1**.

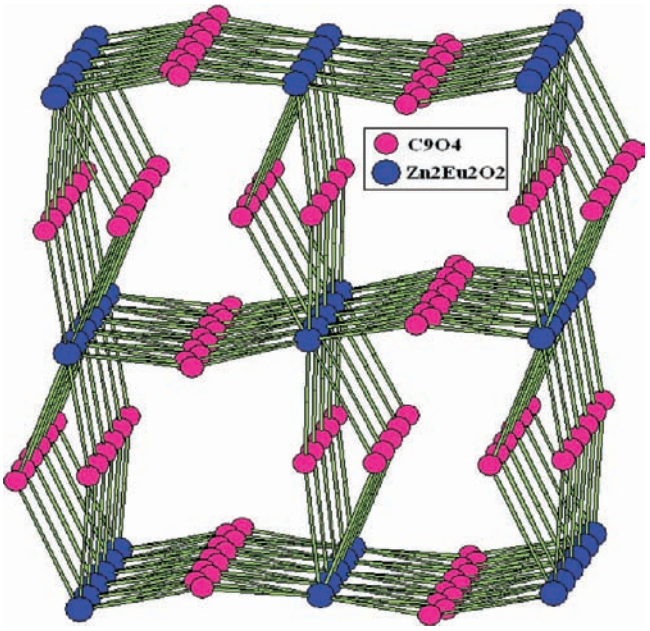

Figure 7. Unusual (2,3,10)-connected 3D topology framework for **Zn−Eu1**.

(labeled with yellow parts in Figure 8b) to entrain a 2D double-layer structure in the *ab* plane as shown in Figure 9a. It is noticeable that the 2D double layer can also be viewed as interlocked subunits. In addition, each subunit is composed of a pair of $Zn_5Eu(OH)$ clusters bridge linked by the carboxylate groups (O−C53−O, O−C46−O, O−C41−O, and O−C37−O) from four mip ligands on a crystallographic inversion center as shown in Figure 9c. Figure 9b shows that all the subunits are connected by carboxylate groups (O−C10−O and O−C16−O) adopting μ_1-η^1:η^1-chelating and μ_2-η^2:η^1-bridging coordination modes (Scheme 1g), resulting in formation of the 1D chain structure. The adjacent chains are further linked by carboxylate groups (O−C34−O and O−C28−O), adopting a μ_2-η^2:η^1-bridging coordination mode (Scheme 1h), into the 2D double-layer structure mentioned above. On the other hand, looking from the *b* axis, the 2D double layers in the *ab* plane can also be viewed as a 1D chain (Figure 10a), which is further interlinked through the carboxylate groups (O−C1−O, O−C8−O, O−C19−O, O−C25−O) from two kinds of mip ligands (labeled with gray and mauve parts in Figure 8a and 8b) to finally generate a 3D framework featuring irregular channels impregnated by parts of the free and coordinated water molecules, as shown in Figure 10b.

From the viewpoint of the topology, the complicated 3D structure of **Zn−Eu2** can also be specified by the point (Schlafli) symbol $(4^{29}.6^{22}.8^{50}.12^4)$ (4^3) $(4^5.6)$ $(4)_4$ as a novel 3D (2,2,2,3,4,15)-connected 6-nodal network as shown in Figure 11 upon considering the mip ligand and the $Zn_5Eu(O)$ cluster as nodes.

FT-IR Spectral Analysis. For the FT-IR spectra of all compounds (Figures S6−S12, Supporting Information) the absorption in the range 3400−3600 cm^{-1} reveals the O−H characteristic stretching vibrations of water molecules and/or hydroxyl groups. In addition, the absence of the characteristic band at around 1700 cm^{-1} indicates complete deprotonation of 5-methoxyisophthalic acid. As a consequence, the characteristic bands of the carboxylate groups are shown in the range 1550−1610 cm^{-1} for the asymmetric stretching vibration $\upsilon_{as}(COO^-)$ and 1360−1420 cm^{-1} for the symmetric stretching vibration $\upsilon_s(COO^-)$. The above results are all consistent with the single-crystal X-ray diffraction studies.

Metal Ions Oxidation State Analysis. It is known that the concept of bond valence sum (BVS) is often applied to solve

dx.doi.org/10.1021/ic201124c |*Inorg. Chem.* 2011, 50, 10163–10177

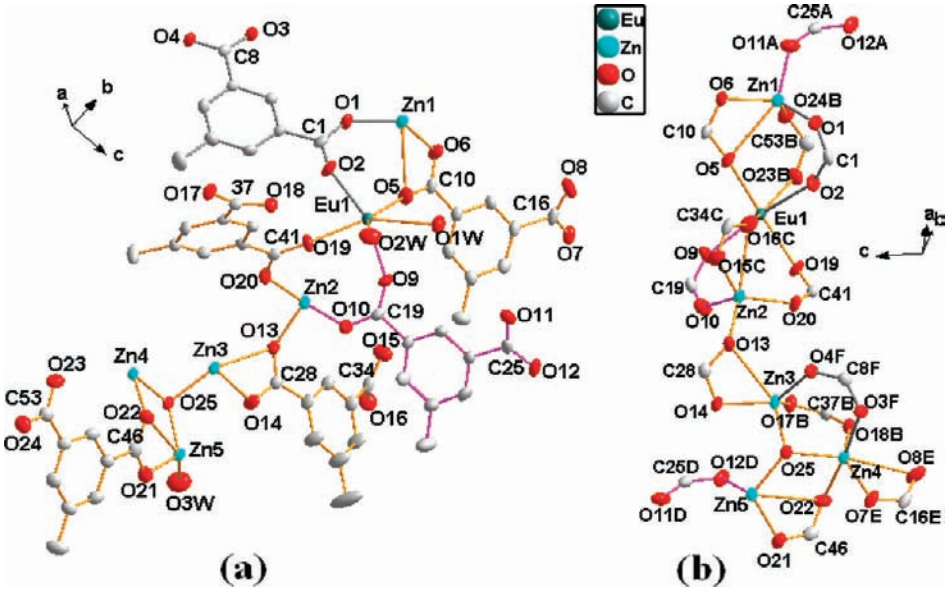

Figure 8. (a) Independent crystallographic unit is shown as thermal ellipsoids (50% probability level) for **Zn**−**Eu2**. (b) Coordination environment of the mip ligand; Zn and Eu atoms are shown as thermal ellipsoids (50% probability level) for **Zn**−**Eu2**. Hydrogen atoms are omitted for clarity. Symmetry codes: A $(2-x, 2-y, 1-z)$, B $(1-x, 1-y, -z)$, C $(2-x, 1-y, 1-z)$, D $(1-x, 1-y, 1-z)$, E $(-1+x, -1+y, -1+z)$, F $(2-x, 1-y, -z)$.

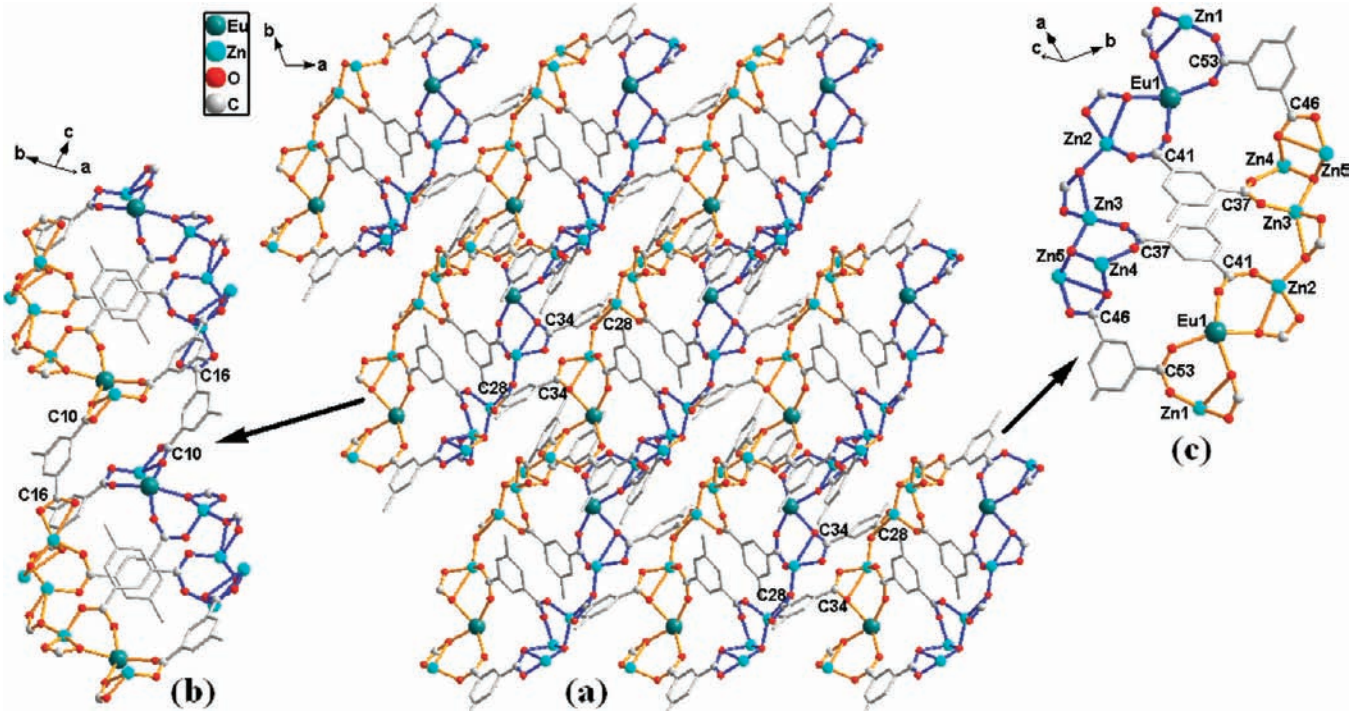

Figure 9. (a) 2D double-layer structure composed of interlocked subunits for **Zn**−**Eu2**. (b) 1D chain structure composed of the subunits and carboxylate groups (O−C10−O and O−C16−O) for **Zn**−**Eu2**. (c) Subunit composed of $Zn_5Eu(OH)$ cluster and carboxylate groups (O−C53−O, O−C46−O, O−C41−O, and O−C37−O) for **Zn**−**Eu2**.

crystal structures of many new materials.[40] The bond valence (S) correlates with the bond length (R) through a relationship which can be expressed as $S = \exp(R_o - R)/B$, where R is the experimentally determined interatomic distance and R_o and B are constants depending on the atoms and given default values by the software Bond Valence Calculator.[41] The BVS values of the cations in all compounds have been tabulated in Table 3 using the software mentioned above. It indicates that the oxidation states of Zn, Mn, Sm, Eu, and Tb atoms should be +2, +2, +3, +3, and +3, respectively, which are consistent with formula of the corresponding compounds. Therefore, the rationality of the corresponding crystal structures was further proved by the BVS values.

Here, it is noticeable that now the oxidation state of Mn is +2, which makes it difficult to distinguish the positions between the

dx.doi.org/10.1021/ic201124c |*Inorg. Chem.* 2011, 50, 10163–10177

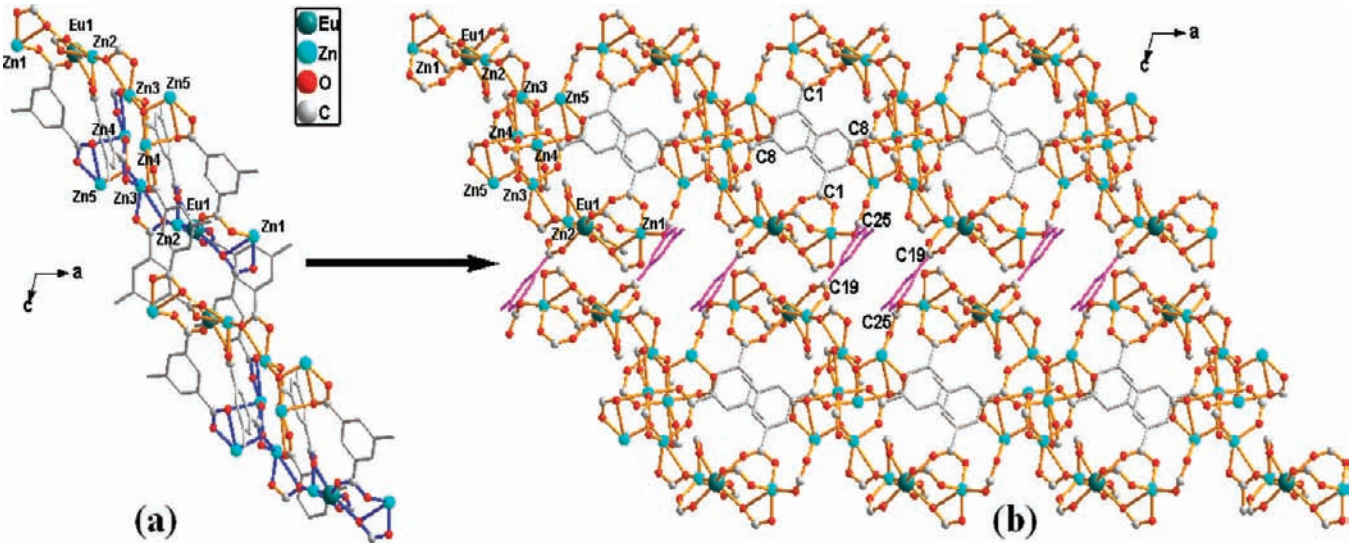

Figure 10. (a) View of the Figure 9a along the *b* axis for **Zn—Eu2**. (b) 3D framework featuring irregular channels for **Zn—Eu2**.

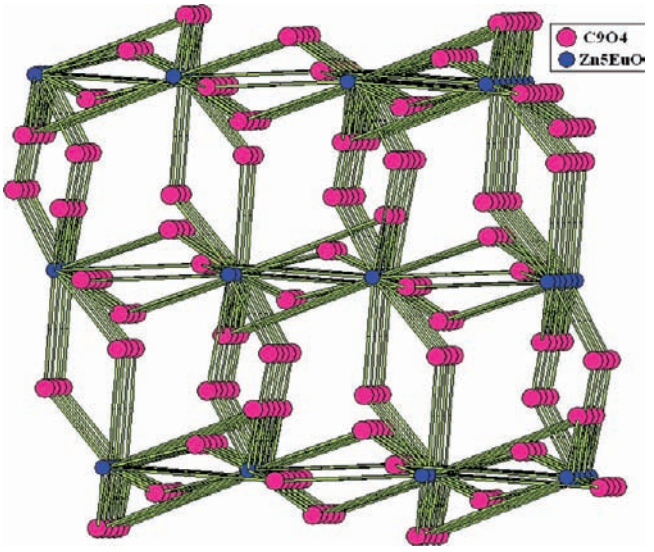

Figure 11. Novel (2,2,2,3,4,15)-connected 3D topology framework for **Zn—Eu2**.

Zn^{2+} and the Mn^{2+} in the previous crystal structure refinement of the compound **Zn—Mn**, since the radius of Zn^{2+} and Mn^{2+} is almost the same (0.80 Å for Mn^{2+}, 0.74 Å for Zn^{2+}). Therefore, compound **Mn—Mn** is fortunately synthesized only using the 5-methylisophthalic acid, $NH_3 \cdot H_2O$, and $MnSO_4 \cdot H_2O$ as the reagents (where zinc acetylacetonate hydrate is absent). This compound has been characterized by single-crystal and powder X-ray diffraction and has been found isostructural to the compound **Zn—Mn**. By comparison, the single-crystal X-ray diffraction data between **Zn—Mn** and **Mn—Mn** together with the X-ray powder diffraction studies on the burning residuals of the corresponding crystal samples the accurate formula of the corresponding compounds are confirmed finally, as discussed below.

TG-DTA and X-ray Powder Diffraction Analyses. In order to investigate the thermal stabilities of the compounds and judge whether or not the Mn^{2+} ions are incorporated into the Zn-based MOFs, TG-DTA and X-ray powder diffraction analyses were performed. It is evident that the thermal decomposition behavior in **Zn—Eu2** and **Zn—Tb** is similar to each other (Figures S13 and S14, Supporting Information). Below 410 °C, accompanied by the endothermal peaks, weight losses of 4.32% and 3.25% are attributed to release of the crystal and/or coordinated waters for **Zn—Eu2** and **Zn—Tb**, respectively. Both are in good agreement with the calculated values (4.40% for **Zn—Eu2**, 3.32% for **Zn—Tb**). With increasing temperature, a tremendous weight loss is observed, which is ascribed to burning of the organic groups from 410 to 550 °C and some of the inorganic compounds produced. The testing results demonstrated clearly that the organic parts in **Zn—Eu2** and **Zn—Tb** are stable below

Table 3. Summary of Calculated Values from BVS for All Compounds

compound	cation	*B*	R_o	BVS
Zn—Zn	Zn1	0.370	1.704	2.074
Zn—Mn	Zn1	0.370	1.704	1.850
	Mn1	0.370	1.790	1.905
Mn—Mn	Mn1	0.370	1.790	1.846
	Mn2	0.370	1.790	2.067
Zn—Sm	Zn1	0.370	1.704	2.070
	Sm1	0.370	2.090	3.138
Zn—Eu1	Zn1	0.370	1.704	1.603
	Eu1	0.370	2.074	3.147
Zn—Eu2	Zn1	0.370	1.704	2.075
	Zn2	0.370	1.704	2.111
	Zn3	0.370	1.704	1.919
	Zn4	0.370	1.704	2.040
	Zn5	0.370	1.704	2.039
	Eu1	0.370	2.074	3.396
Zn—Tb	Zn1	0.370	1.704	2.095
	Zn2	0.370	1.704	2.124
	Zn3	0.370	1.704	2.018
	Zn4	0.370	1.704	2.060
	Zn5	0.370	1.704	2.014
	Tb1	0.370	2.032	3.228

dx.doi.org/10.1021/ic201124c |*Inorg. Chem.* 2011, 50, 10163–10177

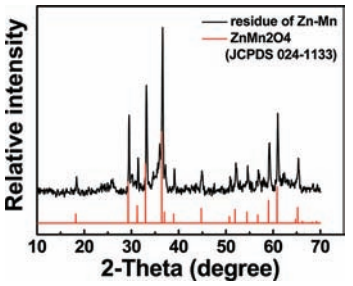

Figure 12. XRPD patterns of the burning residuals for the crystal sample **Zn**−**Mn**, and referenced XRPD patterns for standard sample $ZnMn_2O_4$ (JCPDS 024-1133).

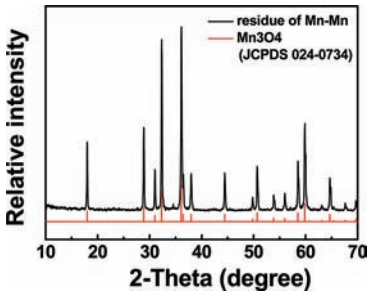

Figure 13. XRPD patterns of the burning residuals for the crystal sample **Mn**−**Mn**, and referenced XRPD patterns for standard sample Mn_3O_4 (JCPDS 024-0734).

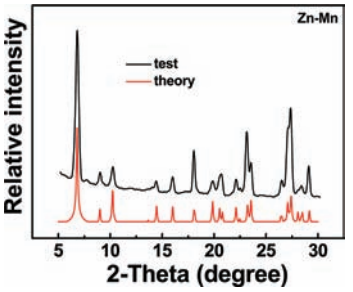

Figure 14. XRPD patterns of the simulated and as-synthesized samples for **Zn**−**Mn**.

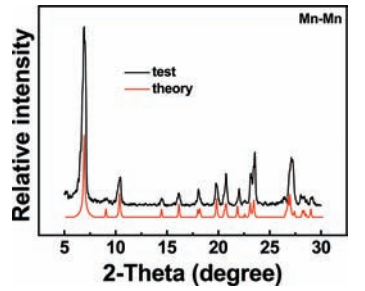

Figure 15. XRPD patterns of the simulated and as-synthesized samples for **Mn**−**Mn**.

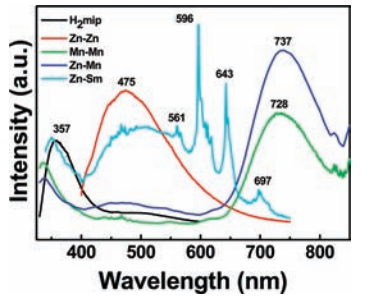

Figure 16. Emission spectra of H2mip, **Zn**−**Zn**, **Mn**−**Mn**, **Zn**−**Mn**, and **Zn**−**Sm** excited at 315, 380, 320, 320, and 310 nm, respectively.

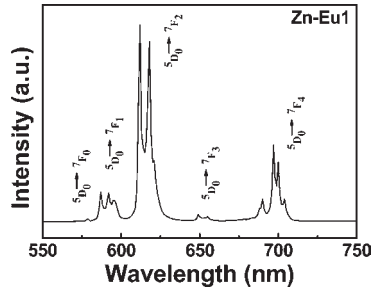

Figure 17. Emission spectrum of **Zn**−**Eu1** excited at 310 nm.

410 °C, which is unusually high for coordination polymers, indicating good thermal stability. Except for compounds **Zn**−**Eu2** and **Zn**−**Tb**, no weight loss was observed from room temperature to 300 °C in the TG-DTA curves of compounds **Zn**−**Zn**, **Zn**−**Mn**, **Mn**−**Mn**, and **Zn**−**Sm** (Figures S15−S18, Supporting Information), which indicates that all of them are anhydrous. Here, it should be noted that both **Zn**−**Mn** and **Mn**−**Mn** show large weight losses with distinctly exothermic peaks corresponding to burning of the organic groups from 300 to 500 °C, which means that the formed frameworks formulated as $[Zn_2Mn(OH)_2(mip)_2]$ and $[Mn_2Mn(OH)_2(mip)_2]$ are all stable below 300 °C. Furthermore, the final residuals taken by the XRPD patterns are attributed to $ZnMn_2O_4$ (JCPDS 024−1133) and Mn_3O_4 (JCPDS 024−0734) for **Zn**−**Mn** and **Mn**−**Mn**, respectively (Figures 12 and 13). On the other hand, as shown in Figures 14 and 15, the X-ray powder diffraction patterns measured for the as-synthesized samples of **Zn**−**Mn** and **Mn**−**Mn** are all in good agreement with the XRPD patterns simulated from the respective single-crystal X-ray data using the Mercury 1.4 program, which proves the purity of the bulk phases. Therefore, the XRPD patterns taken on the burning residuals and as-synthesized samples, metal-ion oxidation state analysis, together with the results of the elemental analysis of **Zn**−**Mn** and **Mn**−**Mn** above further confirm that Mn^{2+} ions are incorporated into the Zn-based MOFs indeed and the compositions of $[Zn_2Mn(OH)_2(mip)_2]$ and $[Mn_2Mn(OH)_2(mip)_2]$ are reasonable.

Photoluminescent Properties. The emission spectra of free ligand H_2mip, **Zn**−**Zn**, **Zn**−**Mn**, **Mn**−**Mn**, and **Zn**−**Sm**, **Zn**−**Eu1**, **Zn**−**Eu2**, and **Zn**−**Tb** in the solid state at room temperature are depicted in Figures 16, 17, 18, and 19, respectively. The excitation spectra are also presented in Figures S19−S24, Supporting Information. It is evident that the fluorescent properties Zn-based MOFs with 5-methylisophthalate ligands are effectively tuned by the Mn^{2+}, Sm^{3+}, Eu^{3+}, and Tb^{3+} ions in hetero-MOFs .

Photoluminescence of the Free Ligand, Zn−**Zn, Zn**−**Mn, Mn**−**Mn, and Zn**−**Sm.** As shown in Figure 16, it can be seen that

dx.doi.org/10.1021/ic201124c |*Inorg. Chem.* 2011, 50, 10163–10177

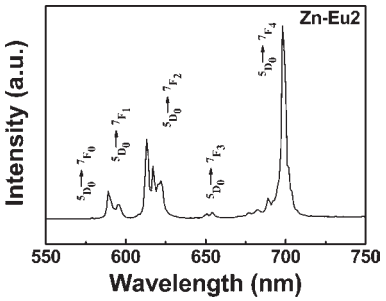

Figure 18. Emission spectrum of **Zn**−**Eu2** excited at 310 nm.

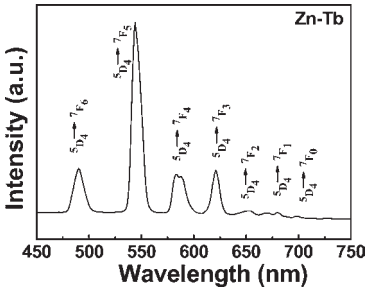

Figure 19. Emission spectrum of **Zn**−**Tb** excited at 312 nm.

H_2mip displays an intense ultraviolet emission at 357 nm upon excitation at 315 nm, which can be assigned to the intraligand fluorescence emission ($\pi-\pi^*$ transitions of the aromatic carboxylic acid). Compared with the intraligand ultraviolet emission of H_2mip, a broad visible emission band at ca. 475 nm (λ_{ex} = 380 nm) for **Zn**−**Zn** should be ascribed to ligand-to-metal charge transfer (LMCT), which is similar to those found for Zn-based MOFs.[17] However, for compound **Zn**−**Mn**, when excited at 320 nm, it exhibited remarkably intense photoluminescence with a deep red color. The obtained emission spectra consist of a strong band centered at 737 nm and a weak broad band ranging from 400 to 600 nm. The former deep red emission band is the characteristic emission of Mn^{2+} corresponding to the $^4T_1 \rightarrow {}^6A_1$ transition, while the latter emission band is attributed to emission of the Zn-based MOFs. To gain insight into the nature of these spectra, we also carry out photoluminescence studies on compound **Mn**−**Mn**. The results show that compound **Mn**−**Mn** exhibited similar Mn^{2+} emissions (λ_{em} = 728 nm, λ_{ex} = 320 nm) with **Zn**−**Mn**, except for a little blue shift due to the different coordination environment around them. Considering the intense emission of Mn^{2+} in **Zn**−**Mn** and the absence of an emission band in **Mn**−**Mn** (400−600 nm), it can be concluded that there only exists negligible energy transfer between the mip ligand and Zn^{2+}. However, it is noted that comparing the emission spectra of compounds **Zn**−**Mn** and **Mn**−**Mn** with the same bandwidth (bandwidth: excitation 3 nm, emission 2 nm), the fluorescence intensity of the deep red emission from Mn^{2+} is enhanced by the presence of Zn^{2+} in the sample. We think it should have originated from Zn^{2+} behaving as an activator for the Mn^{2+} emission, similar to the Mn^{2+}-doped Zn-based host materials, such as the inorganic core/shell microcrystals or inorganic−organic hybrid materials mentioned previously.[15,16] Furthermore, it is worth noting that many of the previously reported Zn−Mn MOFs and Mn-based MOFs are mainly concerned with their magnetic properties.[27−32] Even though several luminescent Mn-based MOFs were investigated by J.-S. Huang and other authors, all of them display the ligand emission finally.[33−38] Therefore, it would be very interesting to investigate the Mn^{2+} emission in the Zn−Mn MOFs and Mn-based MOFs. To our knowledge, compounds **Zn**−**Mn** and **Mn**−**Mn** represent the unique MOFs associated with Mn^{2+} emission ($^4T_1 \rightarrow {}^6A_1$ transition) upon excitation at room temperature, although studies on the same emission of the Mn^{2+}-activated inorganic or inorganic−organic hybrid materials have been widely reported. As for compound **Zn**−**Sm**, it exhibits an orange luminescence when excited at 310 nm and gives a typical Sm^{3+} emission spectrum. The emissions at 561, 596, 643, and 697 nm correspond to the characteristic emission of $^4G_{5/2} \rightarrow {}^6H_{5/2}$, $^4G_{5/2} \rightarrow {}^6H_{7/2}$, $^4G_{5/2} \rightarrow {}^6H_{9/2}$, and $^4G_{5/2} \rightarrow {}^6H_{11/2}$ transitions of the Sm^{3+} ion, respectively. In addition, the peak at 596 nm is the strongest one, which is consistent with those found in previously reported MOFs.[42] However, it should be pointed out that **Zn**−**Sm** also exhibits a relatively intense broad emission band ranging from 400 to 550 nm, which should be assigned to luminescence of the Zn-based MOFs.

Photoluminescence of Zn−Eu1 and Zn−Eu2. Upon excitation at 310 nm, no other emission spectrum except the characteristic emission transition of $^5D_0 \rightarrow {}^7F_J$ (J = 0−4) of the Eu^{3+} ions appears in both **Zn**−**Eu1** and **Zn**−**Eu2** (Figures 17 and 18), indicating ligand-to-zinc energy transfer is inefficient under the experimental conditions. The spectrum of **Zn**−**Eu1** contain $^5D_0 \rightarrow {}^7F_0$ (579 nm), $^5D_0 \rightarrow {}^7F_1$ (587, 592, 596 nm), $^5D_0 \rightarrow {}^7F_2$ (612, 618, 621 nm), $^5D_0 \rightarrow {}^7F_3$ (649, 655 nm), and $^5D_0 \rightarrow {}^7F_4$ (690, 697, 700, 704) transitions. In addition, emission of the transitions of $^5D_0 \rightarrow {}^7F_0$ (579 nm), $^5D_0 \rightarrow {}^7F_1$ (589, 596 nm), $^5D_0 \rightarrow {}^7F_2$ (613, 617, 622 nm), $^5D_0 \rightarrow {}^7F_3$ (651, 654 nm), and $^5D_0 \rightarrow {}^7F_4$ (677, 683, 689, and 699 nm) also appeared in **Zn**−**Eu2**. Furthermore, simultaneous appearance of the symmetry-forbidden emission $^5D_0 \rightarrow {}^7F_0$ in **Zn**−**Eu1** and **Zn**−**Eu2** indicates that all Eu^{3+} ions in the two compounds are located on the site with low symmetry and without an inversion center.[43] This is in agreement with the result of single-crystal structural analysis. Additionally, the $^5D_0 \rightarrow {}^7F_1$ transition is a magnetic dipole one and its intensity varies with the crystal field strength acting on Eu^{3+}, while the $^5D_0 \rightarrow {}^7F_2$ one is an electric dipole transition and is sensitive to chemical bonds in the vicinity of Eu^{3+}. The intensity ratio $I(^5D_0 \rightarrow {}^7F_2)/I(^5D_0 \rightarrow {}^7F_1)$ (6.4 for **Zn**−**Eu1**, 3.0 for **Zn**−**Eu2**) also suggests a noncentrosymmetric coordination environment of the Eu^{3+} ions both in **Zn**−**Eu1** and in **Zn**−**Eu2**. These are all consistent with the result of single-crystal X-ray analysis. However, it is interesting to note that the spectrum of **Zn**−**Eu1** is dominated by the $^5D_0 \rightarrow {}^7F_2$ transition, while emission of the $^5D_0 \rightarrow {}^7F_4$ transition for **Zn**−**Eu2** is the most intense. This phenomenon is quite surprising. To our knowledge, the former is widely observed in the Eu-based MOFs and Eu-activated host materials, while there is no report for the latter except for that by X.-Y. Chen,[44] which showed that Eu^{3+}-doped inorganic nanocrystals (BaFCl) emit the same luminescence bands of the Eu^{3+} ion at 10 K. However, no details on the luminescence properties associated with Eu^{3+}-activated MOFs have been reported yet. A possible explanation for this observation appeared in 3d−4f hetero-MOFs could be that the Eu^{3+} ions in **Zn**−**Eu1** and **Zn**−**Eu2** experience different crystal field strengths, crystal field symmetries, and coordinated bonds with oxygen atoms, which can be distinctly observed from the results of single-crystal X-ray analysis for **Zn**−**Eu1** and **Zn**−**Eu2**.

Therefore, the dual character of the only emission from Eu^{3+} ions and the most intense emission peak centered at 699 nm make compound **Zn−Eu2** have an important significance for developing special Eu^{3+}-activated hetero-MOFs materials.

Photoluminescence of Zn−Tb. Compound **Zn−Tb** emits intense green light when excited at 312 nm and exhibits the characteristic transition of $^5D_4 \rightarrow {}^7F_J$ ($J = 0-6$) of the Tb^{3+} ion (Figure 19) The spectrum is dominated by the $^5D_4 \rightarrow {}^7F_5$ (544 nm) transition, along with $^5D_4 \rightarrow {}^7F_6$ (490 nm), $^5D_4 \rightarrow {}^7F_4$ (583, 588 nm), $^5D_4 \rightarrow {}^7F_3$ (621 nm), $^5D_4 \rightarrow {}^7F_2$ (653 nm), $^5D_4 \rightarrow {}^7F_1$ (671, 679 m), and $^5D_4 \rightarrow {}^7F_0$ (698 nm) transitions, which show agreement with the luminescent Tb^{3+} MOFs reported previously.[45] Furthermore, the absence of the emission coming from Zn-based MOF in the spectrum of **Zn−Tb** also suggests that the energy transfer from the ligand to the Tb^{3+} center is very efficient.

Luminescent Lifetimes and Quantum Efficiencies. The luminescent decay curves by monitoring the most intense emission (λ_{em}) of the respective samples are shown in Figures S25−S31, Supporting Information. It can be seen that the emission decay curves can be well fitted with triexponential functions for **Zn−Zn**, **Zn−Mn**, **Mn−Mn**, **Zn−Sm**, and **Zn−Eu1**. The luminescent lifetimes are as follows: $\tau 1 = 1.85$ ns, $\tau 2 = 5.19$ ns, and $\tau 3 = 17.43$ ns ($\chi^2 = 1.011$, Figure S25, Supporting Information) for **Zn−Zn** ($\lambda_{em} = 475$ nm); $\tau 1 = 3.07$ μs, $\tau 2 = 20.47$ μs, and $\tau 3 = 46.04$ μs ($\chi^2 = 1.151$, Figure S26, Supporting Information) for **Zn−Mn** ($\lambda_{em} = 737$ nm); $\tau 1 = 1.74$ μs, $\tau 2 = 9.12$ μs, and $\tau 3 = 18.81$ μs ($\chi^2 = 1.053$, Figure S27, Supporting Information) for **Mn−Mn** ($\lambda_{em} = 728$ nm); $\tau 1 = 0.54$ μs, $\tau 2 = 7.52$ μs, and $\tau 3 = 27.75$ μs ($\chi^2 = 1.156$, Figure S28, Supporting Information) for **Zn−Sm** ($\lambda_{em} = 596$ nm); $\tau 1 = 0.17$ ms, $\tau 2 = 0.52$ ms, and $\tau 3 = 1.56$ ms ($\chi^2 = 1.158$, Figure S29, Supporting Information) for **Zn−Eu1** ($\lambda_{em} = 612$ nm). For compounds **Zn−Eu2** and **Zn−Tb** their respective emission decay curves obtained can well be fitted biexponentially. In addition, the luminescent lifetimes are $\tau 1 = 0.49$ ms and $\tau 2 = 1.25$ ms ($\chi^2 = 1.160$, Figure S30, Supporting Information) for **Zn−Eu2** ($\lambda_{em} = 699$ nm) and $\tau 1 = 0.69$ ms and $\tau 2 = 1.46$ ms ($\chi^2 = 1.188$, Figure S3, Supporting Information1) for **Zn−Tb** ($\lambda_{em} = 544$ nm), where χ^2 denotes a fit quality parameter for the lifetime data. It can be seen that the luminescence lifetimes fall into the range of the nanosecond (**Zn−Zn**), microsecond (**Zn−Mn**, **Mn−Mn**, and **Zn−Sm**) and millisecond (**Zn−Eu1**, **Zn−Eu2,** and **Zn−Tb**) magnitude orders. Evidently, the Zn-based hetero-MOFs possess a longer lifetime than Zn-based homo-MOF, and Zn-based hetero-MOFs containing europium or terbium also possess a longer lifetime than that of manganese or samarium. On the other hand, we know that the luminescent lifetime is the inverse of the total deactivation rate, which in turn is the sum of the radiative and nonradiative rates. Therefore, it can be concluded that the room-temperature luminescent dynamics properties of the Zn-based MOFs could also be tuned by incorporating RE^{3+} and Mn^{2+} ions into them, similar to tuning the emission band positions mentioned above. Besides, the emission quantum efficiencies of the three most luminescent Zn-based hetero-MOFs, namely, the europium- and the terbium-containing ones, are selectively measured at room temperature. The results show that **Zn−Eu2** possesses the absolute luminescence quantum efficiency of 5%, which is slightly higher than that of **Zn−Eu1** (2%), while **Zn−Tb** displays an exceptionally large emission quantum yield, up to 43%. All these results indicate that the energy transfers from the ligands to the rare earth ions occur in **Zn−Eu1**, **Zn−Eu2**, and **Zn−Tb**. The value of the emission quantum efficiency for **Zn−Eu1** or **Zn−Eu2** is much lower than that of **Zn−Tb**, probably due to the nonradiative losses attributed to multiphonon relaxation.[46] In addition, the energy transfer efficiency in **Zn−Tb** is the biggest among **Zn−Eu1** and **Zn−Eu2**, probably due to a better energy match between the lowest triplet state of the mip ligand and the excited state of Tb^{3+} ion. The detailed energy transfer processes will be discussed in other luminescent mip-bridged MOFs in the future.

CONCLUSION

According to the established methodology of tuning the luminescent properties of the Zn-based inorganic host materials by doping activating metal ions, this paper presents the first successful attempt to tune the photoluminescence properties of Zn-based MOFs by doping different Sm^{3+}, Eu^{3+}, Tb^{3+}, and Mn^{2+} ions in which the structural and photoluminescence properties of seven novel 3D homo- and hetero-MOFs including four kinds of different structures are reported. The results show that the ligand 5-methylisophthalic acid can indeed lead to transition metal or transition metal/lanthanide MOFs with beautiful structures and interesting luminescent properties and without requiring the copresence of other ancillary organic ligands. To the best of our knowledge, compounds **Zn−Sm**, **Zn−Eu1**, **Zn−Eu2**, and **Zn−Tb** are the first 3d−4f hetero-MOFs reported to date using 5-methylisophthalic acid as a single ligand, which provides an example for synthesizing single aromatic carboxylate-bridged 3d−4f hetero-MOFs with new topologies through variation of the other transition metal/lanthanide ions. More importantly, luminescence measurements revealed that compounds **Zn−Mn** and **Mn−Mn** are representatives of the whole family of Mn-based homo- and hetero-MOFs which display an intense emission band corresponding to the characteristic emission of Mn^{2+} ($^4T_1 \rightarrow {}^6A_1$ transition). Therefore, investigation of **Zn−Mn** and **Mn−Mn** opens a new synthetic pathway for the design of novel Mn-based MOFs with potentially luminescent properties. Furthermore, the most intense emission band position centered at 699 nm ($^5D_0 \rightarrow {}^7F_4$ transition) in compound **Zn−Eu2** is also a unique example of all the Eu-based homo- and hetero-MOFs, which make it have important significance for developing special application in the luminescent 3d−4f hetero-MOFs materials. Notably, thanks to incorporating Sm^{3+}, Eu^{3+}, Tb^{3+}, and Mn^{2+} ions into Zn-based MOFs with 5-methylisophthalic acid ligands, the photoluminescence properties of them are easily tuned from the emission band position from 475 (**Zn−Zn**) to 544 (**Zn−Tb**), 596 (**Zn−Sm**), 612 (**Zn−Eu1**), 699 (**Zn−Eu2**), and 737 nm (**Zn−Mn**). In addition, the luminescence lifetimes fall in the range of the nanosecond (**Zn−Zn**), microsecond (**Zn−Mn**, **Mn−Mn**, and **Zn−Sm**), and millisecond (**Zn−Eu1**, **Zn−Eu2**, and **Zn−Tb**) magnitude orders. It indicates that by employing the 5-methylisophthalic acid ligands many structural hetero-MOFs with tunable photoluminescence properties might form, which should be interesting and informative in the rational design of luminescent d−d and d−f hetero-MOFs. Future work will be aimed at the synthesis of other luminescent mip-bridged MOFs and aszsessing the capability of the 5-methylisophthalic acid ligands to act as antenna-type sensitizers for the lanthanide's emission in the visible and near-infrared regions.

EXPERIMENTAL SECTION

General Remarks. All syntheses were performed in poly(tetrafluoroethylene)-lined stainless steel autoclaves under autogenous pressure. Reagents were purchased commercially and used without further purification. Elemental analyses (C and H) were performed on a Perkin-Elmer 2400 Series II CHNS/O elemental analyzer. Zn, Mn, Sm, Eu, and Tb were determined by inductively coupled plasma (ICP) analysis performed on a Perkin-Elmer Optima 3300DV spectrometer. The shape of the samples was observed in a XP-201 optical microscope. IR spectra were recorded in the range 400−4000 cm^{-1} on a Perkin-Elmer FTIR spectrometer using KBr pellets. TG-DTA analyses were performed on a Perkin-Elmer Diamond TG/DTA Instruments in flowing air with a heating rate of 10 °Cmin^{-1}. Solid-state emission and excitation spectra as well as luminescence lifetime measurements were carried out on an Edinburgh FLS920 phosphorimeter equipped with a continuous Xe-900 xenon lamp and an nF900 ns flash lamp. The absolute emission quantum yields of the compounds were measured at room temperature using a calibrated integrating sphere as a sample chamber, and specpure $BaSO_4$ was used as a reflecting standard. X-ray powder diffraction (XRPD) patterns of the samples were recorded on an X-ray diffractometer (Rigaku D/Max 2200PC) with a graphite monochromator and Cu Kα radiation at room temperature, while the voltage and electric current were held at 40 kV and 20 mA. Crystal data of all compounds were collected on a Xcalibur, Eos, Gemini diffractometer (Mo Kα radiation, $\lambda = 0.71073$ Å). Data reduction was accomplished by the CrysAlisPro (Oxford Diffraction Ltd., Version 1.171.33.55) program. Structures were solved by direct methods and refined by a full-matrix least-squares technique based on F^2 using the SHELXL 97 program.[47] All of the non-hydrogen atoms were refined anisotropically. The organic hydrogen atoms were generated geometrically; the aqua hydrogen atoms were located from difference maps and refined with isotropic temperature factors. Drawings of the molecule were performed with the program Diamond.[48] Crystallographic data for the structures reported in this paper have been deposited with the Cambridge Crystallographic Data Centre as supplementary publication nos. CCDC-822111 (**Zn**−**Zn**), CCDC-796515 (**Zn**−**Mn**), CCDC-799369 (**Mn**−**Mn**), CCDC-822109 (**Zn**−**Sm**), CCDC-822105 (**Zn**−**Eu1**), CCDC-822106 (**Zn**−**Eu2**), and CCDC-822110(**Zn**−**Tb**). Copies of the data can be obtained free of charge on application to CCDC, 12 Union Road, Cambridge CB21EZ, U.K. (fax (+44) 1223-336-033; e-mail deposit@ccdc.cam.ac.uk).

Preparation. *Synthesis of* $[Zn(mip)]_n$ (***Zn*−*Zn***). A mixture of zinc acetylacetonate hydrate (1.0 mmol), $NH_3 \cdot H_2O$ (3.0 mmol), and 5-methylisophthalic acid (1.0 mmol) in 15 mL of H_2O was stirred for 10 min at room temperature. The mixture was then transferred into a 30 mL, Teflon-lined stainless-steel vessel. The mixture was heated at 180 °C for 5 days under autogenous pressure. After the reaction mixture was slowly cooled to room temperature, fawn-colored sheet crystals of **Zn**−**Zn** were filtered off, washed with distilled water, and dried in air. Yield: ∼40%. Anal. Calcd for $C_9H_6O_4Zn$: C, 44.39; H, 2.48; Zn, 26.85. Found: C, 44.28; H, 2.39; Zn, 26.77. IR (KBr pellet, cm^{-1}): 3436 s, 2970 w, 2932 w, 2851 w, 1619 s, 1567 s, 1431 m, 1386 s, 1116 w, 1041 m, 929 w, 779 s, 718 m, 584 w, 486 m.

Synthesis of $[Zn_2Mn(OH)_2(mip)_2]_n$ (***Zn*−*Mn***). A mixture of zinc acetylacetonate hydrate (1.0 mmol), $NH_3 \cdot H_2O$ (7.0 mmol), $MnSO_4 \cdot H_2O$ (1.0 mmol), and 5-methylisophthalic acid (2.5 mmol) in 20 mL of H_2O was stirred for 10 min at room temperature. The mixture was then transferred into a 40 mL, Teflon-lined stainless-steel vessel. The mixture was heated at 200 °C for 5 days under autogenous pressure. After the reaction mixture was slowly cooled to room temperature, fawn-colored prism crystals of **Zn**−**Mn** (see Figure S32, Supporting Information) were filtered off, washed with distilled water, and dried in air. Yield: ∼55%. Anal. Calcd for $C_{18}H_{14}O_{10}Zn_2Mn$: C, 37.53; H, 2.45; Zn, 22.70; M_n 9.54. Found: C, 37.48; H, 2.40; Zn, 22.65; M_n 9.46. IR (KBr pellet, cm^{-1}): 3438 s, 2970 w, 2925 w, 2858 w, 1617 s, 1567 s, 1424 m, 1244 w, 1124 w, 1048 w, 951 w, 769 m, 726 m, 620 w, 568 w, 501 w, 456 w.

Synthesis of $[Mn_2Mn(OH)_2(mip)_2]_n$ (***Mn*−*Mn***). A mixture of 5-methylisophthalic acid (1.0 mmol), $NH_3 \cdot H_2O$ (4.0 mmol), and $MnSO_4 \cdot H_2O$ (1.0 mmol) in 20 mL of H_2O was stirred for 10 min at room temperature. The mixture was then transferred into a 40 mL, Teflon-lined stainless-steel vessel. The mixture was heated at 200 °C for 5 days under autogenous pressure. After the reaction mixture was slowly cooled to room temperature, fawn-colored prism crystals of **Mn**−**Mn** were filtered off, washed with distilled water, and dried in air. Yield: ∼40% . Anal. Calcd for $C_{18}H_{14}O_{10}Mn_3$: C, 38.95; H, 2.54, M_n 29.69. Found: C, 38.89; H, 2.51, M_n 29.58 IR (KBr pellet, cm^{-1}): 3451 s, 2925 m, 2858 w, 1609 m, 1566 s, 1439 w, 1416 w, 1386 s, 1363 m, 1306 w, 1245 w, 1119 w, 1049 w, 1018 w, 945 w, 885 m, 768 m, 738 w, 715 m, 608 w, 565 w, 498 w, 448 w.

Synthesis of $[ZnSm(OH)(mip)_2]_n$ (***Zn*−*Sm***). A mixture of zinc acetylacetonate hydrate (1.0 mmol), $NH_3 \cdot H_2O$ (6.0 mmol), $Sm_2(SO_4)_3 \cdot 8H_2O$ (0.50 mmol), and 5-methylisophthalic acid (2.0 mmol) in 20 mL of H_2O was stirred for 10 min at room temperature. The mixture was then transferred into a 40 mL, Teflon-lined stainless-steel vessel. The mixture was heated at 200 °C for 5 days under autogenous pressure. After the reaction mixture was slowly cooled to room temperature, fawn-colored prism crystals of **Zn**−**Sm** were filtered off, washed with distilled water, and dried in air. Yield: ∼75%. Anal. Calcd for $C_{18}H_{13}O_9ZnSm$: C, 36.70; H, 2.22; Zn, 11.10; Sm, 25.53. Found: C, 36.67; H, 2.20; Zn, 11.14; Sm, 25.48. IR (KBr pellet, cm^{-1}): 3586 m, 3428 w, 3091 w, 2918 w, 2858 w, 2527 w, 2385 w, 1829 w, 1627 s, 1562 s, 1432 m, 1365 s, 1322 w, 1255 w, 1142 w, 1115 w, 1042 w, 1002 w, 925 w, 895 w, 845 m, 772 s, 715 s, 668 m, 622 w, 575 w, 528 m, 488 w, 445 w.

Synthesis of $[ZnEu(OH)(mip)_2]_n$ (***Zn*−*Eu1***). Synthesis of **Zn**−**Eu1** was similar to that of **Zn**−**Sm** using $Eu_2(SO_4)_3 \cdot 8H_2O$ instead of $Sm_2(SO_4)_3 \cdot 8H_2O$. After the reaction mixture was slowly cooled to room temperature, fawn-colored prism crystals of **Zn**−**Eu1** were filtered off, washed with distilled water, and dried in air. Yield: ∼55%. Anal. Calcd for $C_{18}H_{13}O_9ZnEu$: C, 36.60; H, 2.22; Zn, 11.07; Eu, 25.73. Found: C, 36.54; H, 2.21; Zn, 11.02; Eu, 25.68. IR (KBr pellet, cm^{-1}): 3579 m, 3451 m, 3091 w, 2925 w, 2867 w, 1822 w, 1627 s, 1567 s, 1432 m, 1369 s, 1319 w, 1249 w, 1115 w, 925 w, 892 w, 848 m, 775 s, 718 s, 665 m, 622 w, 575 w, 528 m, 492 w, 445 w.

Synthesis of $[Zn_5Eu(OH)(H_2O)_3(mip)_6 \cdot (H_2O)]_n$ (***Zn*−*Eu2***). A mixture of zinc acetylacetonate hydrate (1.5 mmol), $NH_3 \cdot H_2O$ (7.5 mmol), $Eu_2(SO_4)_3 \cdot 8H_2O$ (0.75 mmol) and 5-methylisophthalic acid (2.5 mmol) in 20 mL H_2O were stirred for 10 min at room temperature. The mixture is then transferred into a 40 mL, Teflon-lined stainless-steel vessel. The mixture was heated at 210 °C for 5 days under autogenously pressure. After the reaction mixture was slowly cooled to room temperature, fawn-colored prism crystals of **Zn**−**Eu2** were filtered off, washed with distilled water, and dried in air. Yield: ∼50%. Anal. Calcd for $C_{54}H_{45}O_{29}Zn_5Eu$: C, 39.62; H, 2.77; Zn, 19.97; Eu, 9.28. Found: C, 39.56; H, 2.73; Zn, 19.91; Eu, 9.32. IR (KBr pellet, cm^{-1}): 3447 m, 3072 w, 2920 w, 2863 w, 2351 w, 1839 w, 1620 s, 1592 w, 1563 s, 1421 m, 1380 s, 1253 w, 1191 w, 1015 w, 927 w, 891 w, 771 s, 744 w, 717 m, 641 w, 503 w, 459 w.

Synthesis of $[Zn_5Tb(OH)(H_2O)_3(mip)_6]_n$ (***Zn*−*Tb***). Synthesis of **Zn**−**Tb** was similar to that of **Zn**−**Eu2** using $Tb_2(SO_4)_3 \cdot 8H_2O$ instead of $Eu_2(SO_4)_3 \cdot 8H_2O$. After the reaction mixture was slowly cooled to room temperature, fawn-colored prism crystals of **Zn**−**Tb** were filtered off, washed with distilled water, and dried in air. Yield: ∼45%. Anal. Calcd for $C_{54}H_{43}O_{28}Zn_5Tb$: C, 39.89; H, 2.67; Zn, 20.11; Tb, 9.78. Found: C, 39.82; H, 2.63; Zn, 20.08; Tb, 9.71. IR (KBr pellet, cm^{-1}): 3443 m, 3376 w, 3068 w, 2925 w, 2858 w, 2355 w, 1830 w, 1623 s, 1588 w, 1559 s, 1426 m, 1386 s, 1249 w, 1192 w, 1112 w, 1008 w, 935 w, 898 w, 775 s, 745 w, 722 m, 645 w, 498 w, 465 w.

■ ASSOCIATED CONTENT

Supporting Information. X-ray crystallographic data in CIF format, selected bond distances and angles, coordination environment of the mip ligand and Zn, Mn, Sm, Eu, and Tb atoms, TG-DTA curves, excitation spectra, FT-IR spectra, luminescent lifetime decay profiles, micrographs of the fawn-colored prism crystals for **Zn**−**Mn**. This material is available free of charge via the Internet at http://pubs.acs.org.

■ AUTHOR INFORMATION

Corresponding Author
*E-mail: chm_boqb@ujn.edu.cn.

■ ACKNOWLEDGMENT

We gratefully acknowledge financial support by the Shandong Provincial Natural Science Foundation of China (grant no. ZR2010BM036) and the National Natural Science Foundation of China (grant no. 21171068).

■ REFERENCES

(1) (a) Badalawa, W.; Matsui, H.; Osone, T.; Hasuike, N.; Harima, H.; Tabata, H. *J. Appl. Phys.* **2011**, *109*, 053502. (b) Ji, S.-L.; Yin, L.-L.; Liu, G.-D.; Zhang, L.-D.; Ye, C.-H. *J. Phys. Chem. C* **2009**, *113*, 16439. (c) Wang, M.-L.; Huang, C.-G.; Huang, Z.; Guo, W.; Huang, J.-Q.; He, H.; Wang, H.; Cao, Y.-G.; Liu, Q.-L.; Liang, J.-K. *Opt. Mater.* **2009**, *31*, 1502. (d) Ji, S.-L.; Yin, L.-L.; Liu, G.-D.; Zhang, L.-D.; Ye, C.-H. *Chem. Commun.* **2009**, *17*, 2344. (e) Li, G.-R.; Dawa, C.-R.; Lu, X.-H.; Yu, X.-L.; Tong, Y.-X. *Langmuir* **2009**, *25*, 2378. (f) Du, Y.-P.; Zhang, Y.-W.; Sun, L.-D.; Yan, C.-H. *J. Phys. Chem. C* **2008**, *112*, 12234. (g) Armelao, L.; Bottaro, G.; Pascolini, M.; Sessolo, M.; Tondello, E.; Bettinelli, M.; Speghini, A. *J. Phys. Chem. C* **2008**, *112*, 4049. (h) Zeng, X.; Yuan, J.; Wang, Z.; Zhang, L. *Adv. Mater.* **2007**, *19*, 4510.

(2) Tanaka, M.; Kurita, A.; Yamada, H.; Akimoto, K. *Solid State Commun.* **2007**, *142*, 36.

(3) Purohit, P. J.; Mohapatra, M.; Natarajan, V.; Godbole, S. V. *J. Mater. Sci.* **2011**, *46*, 2030.

(4) Blasse, G.; Grabmaier, B. C. *Luminescent Materials*; Springer: Berlin, 1994.

(5) Li, W.-W.; Yu, W.-L.; Jiang, Y.-J.; Jing, C.-B.; Zhu, J.-Y.; Zhu, M.; Hu, Z.-G.; Tang, X.-D.; Chu, J.-H. *J. Phys. Chem. C* **2010**, *114*, 11951.

(6) (a) Hoa, T. T. Q.; The, N. D.; McVitie, S.; Nam, N. H.; Vu, L. V.; Canh, T. D.; Long, N. N. *Opt. Mater.* **2011**, *33*, 308. (b) Quan, Z.-W.; Wang, Z.-L.; Yang, P.-P.; Lin, J.; Fang, J.-Y. *Inorg. Chem.* **2007**, *46*, 1354. (c) Li, P.; Wang, L.-Y.; Wang, L.; Li, Y.-D. *Chem.—Eur. J.* **2008**, *14*, 5951. (d) Murugadoss, G.; Rajamannan, B.; Ramasamy, V. *J. Lumin.* **2010**, *130*, 2032. (e) Goudarzi, A.; Aval, G. M.; Park, S. S.; Choi, M.-C.; Sahraei, R.; Ullah, M. H.; Avane, A.; Ha, C.-S. *Chem. Mater.* **2009**, *21*, 2375.

(7) (a) Mahamuni, S.; Lad, A. D.; Patole, S. *J. Phys. Chem. C* **2008**, *112*, 2271. (b) Irvine, S. E.; Staudt, T.; Rittweger, E.; Engelhardt, J.; Hell, S. W. *Angew. Chem., Int. Ed.* **2008**, *47*, 2685.

(8) Bhattacharyya, S.; Zitoun, D.; Estrin, Y.; Moshe, O.; Rich, D. H.; Gedanken, A. *Chem. Mater.* **2009**, *21*, 326.

(9) (a) Wang, L.-L.; Liu, X.-M.; Hou, Z.-Y.; Li, C.-X.; Yang, P.-P.; Cheng, Z.-Y.; Lian, H.-Z.; Lin, J. *J. Phys. Chem. C* **2008**, *112*, 18882. (b) An, J.-S.; Noh, J. H.; Cho, I.-S.; Roh, H.-S.; Kim, J. Y.; Han, H. S.; Hong, K. S. *J. Phys. Chem. C* **2010**, *114*, 10330.

(10) Duan, C. J.; Delsing, A. C. A.; Hintzen, H. T. *Chem. Mater.* **2009**, *21*, 1010.

(11) Pires, A. M.; Davolos, M. R. *Chem. Mater.* **2001**, *13*, 21.

(12) Mall, M.; Kumar, L. *J. Lumin.* **2010**, *130*, 660.

(13) Liu, Y.-Y.; Zou, Z.-S.; Liang, X.-L.; Wang, S.-F.; Xing, Z.-W.; Chen, G.-R. *J. Am. Ceram. Soc.* **2010**, *93*, 1891.

(14) Kubota, S.; Oyama, T.; Yamane, H.; Shimada, M. *Chem. Mater.* **2003**, *15*, 3403.

(15) (a) Zhu, D.; Jiang, X.-X.; Zhao, C.-E.; Sun, X.-L.; Zhang, J.-R.; Zhu, J.-J. *Chem. Commun.* **2010**, *46*, 5226. (b) Zheng, J.-J.; Yuan, X.; Ikezawa, M.; Jing, P.-T.; Liu, X.-Y.; Zheng, Z.-H.; Kong, X.-G.; Zhao, J.-L.; Masumoto, Y. *J. Phys. Chem. C* **2009**, *113*, 16969.

(16) (a) Zhang, M.; Shi, C.; Zhang, T.-K.; Feng, M.; Chang, L.; Yao, W.-T.; Yu, S.-H. *Chem. Mater.* **2009**, *21*, 5485. (b) He, Y.; Wang, H.-F.; Yan, X.-P. *Chem.—Eur. J.* **2009**, *15*, 5436. (c) Singleton, R.; Bye, J.; Dyson, J.; Baker, G.; Ranson, R. M.; Hix, G. B. *Dalton Trans.* **2010**, *39*, 6024.

(17) (a) Barbieri, A.; Accorsi, G.; Armaroli, N. *Chem. Commun.* **2008**, 2185. (b) Zheng, S.-L.; Chen, X.-M. *Aust. J. Chem.* **2004**, *57*, 703. (c) Erxleben, A. *Coord. Chem. Rev.* **2003**, *246*, 203.

(18) (a) Zang, S.-Q.; Liang, R.; Fan, Y.-J.; Hou, H.-W.; Mak, T. C. W. *Dalton Trans.* **2010**, *39*, 8022. (b) Xu, J.-Y.; Xie, C.-Z.; Xue, F.; Hao, L.-F.; Ma, Z.-Y.; Liao, D.-Z.; Yan, S.-P. *Dalton Trans.* **2010**, *39*, 7159. (c) Jin, J.-C.; Zhang, Y.-N.; Wang, Y.-Y.; Liu, J.-Q.; Dong, Z.; Shi, Q.-Z. *Chem. Asian J.* **2010**, *5*, 1611. (d) Chen, L.; Xu, G.-J.; Shao, K.-Z.; Zhao, Y.-H.; Yang, G.-S.; Lan, Y.-Q.; Wang, X.-L.; Su, Z.-M. *CrystEngComm* **2010**, *12*, 2157. (e) Ma, L.-F.; Li, C.-P.; Wang, L.-Y.; Du, M. *Cryst. Growth Des.* **2010**, *10*, 2641. (f) Hua, Q.; Zhao, Y.; Xu, G.-C.; Chen, M.-S.; Su, Z.; Cai, K.; Sun, W.-Y. *Cryst. Growth Des.* **2010**, *10*, 2553. (g) Yang, G.-P.; Wang, Y.-Y.; Zhang, W.-H.; Fu, A.-Y.; Liu, R.-T.; Lermontova, E. K.; Shi, Q.-Z. *CrystEngComm* **2010**, *12*, 1509. (h) Yang, J.; Wu, B.; Zhuge, F.; Liang, J.; Jia, C.; Wang, Y.-Y.; Tang, N.; Shi, Q.-Z. *Cryst. Growth Des.* **2010**, *10*, 2331. (i) Zeng, F.; Ni, J.; Wang, Q.; Ding, Y.; Ng, S. W.; Zhu, W.; Xie, Y. *Cryst. Growth Des.* **2010**, 10. (j) Huang, F.-P.; Tian, J.-L.; Chen, G.-J.; Li, D.-D.; Gu, W.; Liu, X.; Yan, S.-P.; Cheng, P. *CrystEngComm* **2010**, *12*, 1269. (k) Kang, J.-G.; Shin, J.-S.; Cho, D.-H.; Jeong, Y.-K.; Park, C.; Soh, S. F.; Lai, C. S.; Tiekink, E. R. T. *Cryst. Growth Des.* **2010**, *10*, 1247. (l) Zhang, L.-P.; Ma, J.-F.; Yang, J.; Pang, Y.-Y.; Ma, J.-C. *Inorg. Chem.* **2010**, *49*, 1535. (m) Habib, H. A.; Hoffmann, A.; Hopped, H. A.; Sieinfeld, G.; Janiak, C. *Inorg. Chem.* **2009**, *48*, 2166.

(19) Lu, W.-G.; Jiang, L.; Feng, X.-L.; Lu, T.-B. *Inorg. Chem.* **2009**, *48*, 6997.

(20) (a) Zhao, S.-S.; Lu, X.-Q.; Hou, A.-X.; Wong, W.-Y.; Wong, W.-K.; Yang, X.-P.; Jones, R. A. *Dalton Trans.* **2009**, 9595. (b) Wang, H.-L.; Zhang, D.-P.; Ni, Z.-H.; Li, X.-Y.; Tian, L.-J.; Jiang, J.-Z. *Inorg. Chem.* **2009**, *48*, 5946. (c) Wei, T.; Zhao, S.-S.; Bi, W.-Y.; Lü, X.-Q.; Hui, Y.-N.; Song, J.-R.; Wong, W.-K.; Jones, R. A. *Inorg. Chem. Commun.* **2009**, *12*, 1216. (d) Bi, W.-Y.; Wei, T.; Lu, X.-Q.; Hui, Y.-N.; Song, J.-R.; Zhao, S.-S.; Wong, W.-K.; Jones, R. A. *New J. Chem.* **2009**, 33, 2326. (e) Feng, W.-X.; Hui, Y.-N.; Wei, T.; Lü, X.-Q.; Song, J.-R.; Chen, Z.-N.; Zhao, S.-S.; Wong, W.-K.; Jones, R. A. *Inorg. Chem. Commun.* **2011**, *14*, 75. (f) Lu, X.-Q.; Bi, W.-Y.; Chai, W.-L.; Song, J.-R.; Meng, J.-X.; Wong, W.-Y.; Wong, W.-K.; Jones, R. A. *New J. Chem.* **2008**, *32*, 127. (g) Lü, X.-Q.; Feng, W.-X.; Hui, Y.-N.; Wei, T.; Song, J.-R.; Zhao, S.-S.; Wong, W.-Y.; Wong, W.-K.; Jones, R. A. *Eur. J. Inorg. Chem.* **2010**, 2714. (h) Akine, S.; Utsuno, F.; Taniguchi, T.; Nabeshima, T. *Eur. J. Inorg. Chem.* **2010**, 3143. (i) Pasatoiu, T. D.; Madalan, A. M.; Kumke, M. U.; Tiseanu, C.; Andruh, M. *Inorg. Chem.* **2010**, *49*, 2310. (j) Hui, Y.-N.; Feng, W.-X.; Wei, T.; Lü, X.-Q.; Song, J.-R.; Zhao, S.-S.; Wong, W.-K.; Jones, R. A. *Inorg. Chem. Commun.* **2011**, *14*, 200. (k) Bi, W.-Y.; Lü, X.-Q.; Chai, W.-L.; Wei, T.; Song, J.-R.; Zhao, S.-S.; Wong, W.-K. *Inorg. Chem. Commun.* **2009**, *12*, 267.

(21) Li, Z.-Y.; Dai, J.-W.; Qiu, H.-H.; Yue, S.-T.; Liu, Y.-L. *Inorg. Chem. Commun.* **2010**, *13*, 452.

(22) (a) Chen, L.; Lin, X.-M.; Ying, Y.; Zhan, Q.-G.; Hong, Z.-H.; Li, J.-Y.; Weng, N. S.; Cai, Y.-P. *Inorg. Chem. Commun.* **2009**, *12*, 761. (b) Song, Y.-S.; Yan, B.; Weng, L.-H. *Inorg. Chem. Commun.* **2006**, *9*, 567. (c) He, R.; Liang, Q.; Song, H.-H.; Wei, Z. *Struct. Chem.* **2010**, *21*, 923. (d) Chi, Y.-X.; Niu, S.-Y.; Jin, J. *Inorg. Chim. Acta* **2009**, *362*, 3821.

(23) (a) Lü, X.-Q.; Bi, W.-Y.; Chai, W.-L.; Song, J.-R.; Meng, J.-X.; Wong, W.-Y.; Wong, W.-K.; Yang, X.-P.; Jones, R. A. *Polyhedron* **2009**, *28*, 27. (b) Bai, Y.-Y.; Huang, Y.; Yan, B.; Song, Y.-S.; Weng, L.-H. *Inorg. Chem. Commun.* **2008**, *11*, 1030. (c) Yin, M.-C.; Sun, J.-T. *J. Coord. Chem.* **2005**, *58*, 335.

(24) (a) Wang, Y.; Cheng, P.; Chen, J.; Liao, D.-Z.; Yan, S.-P. *Inorg. Chem.* **2007**, *46*, 4530. (b) Wang, Y.; Fang, M.; Li, Y.; Liang, J.; Shi, W.; Chen, J.; Cheng, P. *Int. J. Hydrogen Energy* **2010**, *35*, 8166.
(25) Gao, H.-L.; Zhao, B.; Zhao, X.-Q.; Song, Y.; Cheng, P.; Liao, D.-Z.; Yan, S.-P. *Inorg. Chem.* **2008**, *47*, 11057.
(26) Yin, M.-C.; Lei, X.-F.; Li, M.-L.; Yuan, L.-J.; Sun, J.-T. *J. Phys. Chem. Solids* **2006**, *67*, 1372.
(27) Clegg, W.; Little, I. R.; Straughan, B. P. *Inorg. Chem.* **1998**, *27*, 1916.
(28) Dawe, L. N.; Shuvaev, K. V.; Thompson, L. K. *Inorg. Chem.* **2009**, *48*, 3323.
(29) Feng, P. L.; Koo, C.; Henderson, J. J.; Manning, P.; Nakano, M.; Barco, E. D.; Hill, S.; Hendrickson, D. N. *Inorg. Chem.* **2009**, *48*, 3480.
(30) Feng, P. L.; Beedle, C. C.; Wernsdorfer, W.; Koo, C.; Nakano, M.; Hill, S.; Hendrickson, D. N. *Inorg. Chem.* **2007**, *46*, 8126.
(31) Feng, P. L.; Koo, C.; Henderson, J. J.; Nakano, M.; Hill, S.; Barco, E. D.; Hendrickson, D. N. *Inorg. Chem.* **2008**, *47*, 8610.
(32) Ren, P.; Shi, W.; Cheng, P. *Cryst. Growth Des.* **2008**, *8*, 1097.
(33) Liu, G.-N.; Guo, G.-C.; Wang, M.-S.; Cai, L.-Z.; Huang, J.-S. *J. Mol. Struct.* **2010**, *983*, 104.
(34) Fu, M.-L.; Guo, G.-C.; Cai, L.-Z.; Zhang, Z.-J.; Huang, J.-S. *Inorg. Chem.* **2005**, *44*, 184.
(35) Fu, M.-L.; Guo, G.-C.; Liu, X.; Zou, J.-P.; Xu, G.; Huang, J.-S. *Cryst. Growth Des.* **2007**, *7*, 2387.
(36) Pan, Z.-R.; Song, Y.; Jiao, Y.; Fang, Z.-J.; Li, Y.-Z.; Zheng, H.-G. *Inorg. Chem.* **2008**, *47*, 5162.
(37) Roy, A. S.; Biswas, M. K.; Weyhermuller, T.; Ghosh, P. *Dalton Trans.* **2011**, *40*, 146.
(38) Fu, M.-L.; Guo, G.-C.; Liu, X.; Chen, W.-T.; Liu, B.; Huang, J.-S. *Inorg. Chem.* **2006**, *45*, 5793.
(39) (a) Zhou, D.-S.; Wang, F.-K.; Yang, S.-Y.; Xie, Z.-X.; Huang, R.-B. *CrystEngComm* **2009**, *11*, 2548. (b) Ma, L.-F.; Wang, L.-Y.; Hu, J.-L.; Wang, Y.-Y.; Yang, G.-P. *Cryst. Growth. Des.* **2009**, *9*, 5334. (c) Ma, L.-F.; Li, B.; Sun, X.-Y.; Wang, L.-Y.; Fan, Y.-T. *Z. Anorg. Allg. Chem.* **2010**, *636*, 1606.
(40) Brown, I. D. *Acta Crystallogr.* **1977**, *B33*, 1305.
(41) Hormillosa, C.; Healy, S. *Bond Valence Calculator*, version 2.0; McMaster University: Hamilton, Canada, 1993.
(42) (a) Bo, Q.-B.; Sun, G.-X.; Geng, D.-L. *Inorg. Chem.* **2010**, *49*, 561. (b) Ren, Y.-X.; Zhang, M.-L.; Li, D.-S.; Fu, F.; Wang, J.-J.; Du, M.; Hou, X.-Y.; Wu, Y.-P. *Inorg. Chem. Commun.* **2011**, *14*, 231.
(43) Bünzli, J. C. G.; Piguet, C. *Chem. Soc. Rev.* **2005**, *34*, 1048.
(44) Ju, Q.; Liu, Y.-S.; Li, R.-F.; Liu, L.-Q.; Luo, W.-Q.; Chen, X.-Y. *J. Phys. Chem. C* **2009**, *113*, 2309.
(45) (a) Lucky, M. V.; Sivakumar, S.; Reddy, M. L. P.; Paul, A. K.; Natarajan, S. *Cryst. Growth. Des.* **2011**, *11*, 857. (b) Sun, Y.-G.; Wu, Y.-L.; Xiong, G.; Smet, P. F.; Ding, F.; Guo, M.-Y.; Zhu, M.-C.; Gao, E.-J.; Poelman, D.; Verpoort, F. *Dalton Trans.* **2010**, *39*, 11383. (c) Rocha, J.; Carlos, L. D.; Paza, F. A. A.; Ananiasab, D. *Chem. Soc. Rev.* **2011**, *40*, 926.
(46) Bassett, A. P.; Magennis, S. W.; Glover, P. B.; Lewis, D. J.; Spencer, N.; Parsons, S.; Williams, R. M.; Cola, L. D.; Pikramenou, Z. *J. Am. Chem. Soc.* **2004**, *126*, 9413.
(47) (a) Sheldrick, G. M. *SHELXL-97*; University of Göttingen: Göttingen, Germany, 1997. (b) Sheldrick, G. M. *Acta Crystallogr., Sect. A* **2008**, *64*, 112.
(48) Brandenburg, K. *DIAMOND-Crystal and Molecular Structure Visualization*; Crystal Impact GbR: Bonn, Germany, 2010.